Molecular Plant
Resource Article

CellPress
Partner Journal

Reshaping of the *Arabidopsis thaliana* Proteome Landscape and Co-regulation of Proteins in Development and Immunity

Mona Bassal[1,7], Mohammad Abukhalaf[1,7], Petra Majovsky[1,2], Domenika Thieme[1], Tobias Herr[1], Mohamed Ayash[1], Naheed Tabassum[1,3], MHD Rami Al Shweiki[1,4], Carsten Proksch[1], Ali Hmedat[1,5], Jörg Ziegler[1,6], Justin Lee[1], Steffen Neumann[1] and Wolfgang Hoehenwarter[1,*]

[1]Leibniz Institute of Plant Biochemistry, Biochemistry of Plant Interactions Department, Proteome Biology of Plant Interactions Research Group, Weinberg 3, Halle/Saale D-06120, Germany

[2]Present address: Früh Verpackungstechnik AG, Fehrarltorf, Switzerland

[3]Present address: King Abdullah University of Science and Technology, Thuwal, Saudi Arabia

[4]Present address: Ulm University, Ulm, Germany

[5]Present address: Universitätsklinikum Halle (Saale), Sektion Tumorbiologie, Halle/Saale, Germany

[6]Present address: Molecular Signal Integration Department, Halle, Germany

[7]These authors contributed equally to this article.

***Correspondence: Wolfgang Hoehenwarter (wolfgang.hoehenwarter@ipb-halle.de)**

https://doi.org/10.1016/j.molp.2020.09.024

ABSTRACT

Proteome remodeling is a fundamental adaptive response, and proteins in complexes and functionally related proteins are often co-expressed. Using a deep sampling strategy we define core proteomes of *Arabidopsis thaliana* tissues with around 10 000 proteins per tissue, and absolutely quantify (copy numbers per cell) nearly 16 000 proteins throughout the plant lifecycle. A proteome-wide survey of global post-translational modification revealed amino acid exchanges pointing to potential conservation of translational infidelity in eukaryotes. Correlation analysis of protein abundance uncovered potentially new tissue- and age-specific roles of entire signaling modules regulating transcription in photosynthesis, seed development, and senescence and abscission. Among others, the data suggest a potential function of RD26 and other NAC transcription factors in seed development related to desiccation tolerance as well as a possible function of cysteine-rich receptor-like kinases (CRKs) as ROS sensors in senescence. All of the components of ribosome biogenesis factor (RBF) complexes were found to be co-expressed in a tissue- and age-specific manner, indicating functional promiscuity in the assembly of these less-studied protein complexes in *Arabidopsis*.Furthermore, we characterized detailed proteome remodeling in basal immunity by treating *Arabidopsis* seeldings with flg22. Through simultaneously monitoring phytohormone and transcript changes upon flg22 treatment, we obtained strong evidence of suppression of jasmonate (JA) and JA-isoleucine (JA-Ile) levels by deconjugation and hydroxylation by IAA-ALA RESISTANT3 (IAR3) and JASMONATE-INDUCED OXYGENASE 2 (JOX2), respectively, under the control of JASMONATE INSENSITIVE 1 (MYC2), suggesting an unrecognized role of a new JA regulatory switch in pattern-triggered immunity. Taken together, the datasets generated in this study present extensive coverage of the *Arabidopsis* proteome in various biological scenarios, providing a rich resource available to the whole plant science community.

Key words: *Arabidopsis*, deep proteomics, protein co-expression, plant immunity, jasmonate

Bassal M., Abukhalaf M., Majovsky P., Thieme D., Herr T., Ayash M., Tabassum N., Al Shweiki M.R., Proksch C., Hmedat A., Ziegler J., Lee J., Neumann S., and Hoehenwarter W. (2020). Reshaping of the *Arabidopsis thaliana* Proteome Landscape and Co-regulation of Proteins in Development and Immunity. Mol. Plant. **13**, 1709–1732.

Published by the Molecular Plant Shanghai Editorial Office in association with Cell Press, an imprint of Elsevier Inc., on behalf of CSPB and IPPE, CAS.

INTRODUCTION

Proteome biology has received increasing interest in the last few years but still proves difficult on a genome-wide scale in plants. The proteome is the most fundamental active determinant of an organism's phenotype, and its landscape is large, complex, and dynamic, entailing changes in protein abundance, interaction, post-translational modification (PTM), and sub-cellular localization.

Steady-state protein abundance at a certain time point is to a considerable part determined by the abundance of its transcript and the latter's translation rate. Synthesis is, however, only half of the equation governing protein abundance; indeed, *Arabidopsis* has more than 600 F-box proteins serving as components of diverse E3 ubiquitin ligase complexes that direct protein degradation. Newer evidence has shown that post-transcriptional and translational mechanisms (Ponnala et al., 2014; Merchante et al., 2017) and phenomena, such as cell-to-cell mobile mRNAs (Thieme et al., 2015) and proteins (Han et al., 2014; Guan et al., 2017), play equally important roles in determining the proteome's temporal and spatial plasticity foremost in steady-state shifts. Therefore, despite the continued practice of quantifying the abundance of proteins' cognate transcripts to estimate and quantify functional protein coding gene expression, direct, large-scale measurement of protein abundance and PTM should be the explicit endpoint of functional genomics.

However, the problem is that proteomics has long been beset by a lack of sensitivity, especially in plants. To date, only a handful of true deep proteomics studies in plants can be found. Walley et al. (2016) constructed a protein co-expression network based on measurement of 17 862 proteins and 6227 phosphorylated proteins in maize. The tissue- and development-specific wheat proteome has been mapped with measurement of 15 779 proteins (Duncan et al., 2017), and in the tomato fruit 7738 proteins were measured in one or more developmental stages (Szymanski et al., 2017). Song et al. (2018) reported optimized FASP sample preparation in conjunction with two-dimensional liquid chromatography-tandem mass spectrometry (LC-MS/MS), which allowed measurement of 11 690 proteins from a single *Arabidopsis* leaf sample, and Baerenfaller et al. (2008) reported the measurement of nearly 15 000 *Arabidopsis* proteins more than 10 years ago.

Recently, two studies reported tissue-specific proteome remodeling during *Arabidopsis* development in unprecedented resolution and detail. Zhang et al. (2019) reported a library of 15 514 proteins from 10 organs of the model plant, which was then used to analyze differential protein abundance under abscisic acid (ABA) stimulus. Earlier this year, a tissue-specific expression atlas comprising 18 210 proteins and 43 903 phosphorylation sites in 30 tissues was published (Mergner et al., 2020), concomitantly with the initial post of our work in bioRxiv.

We quantified nearly 16 000 proteins in absolute terms (copy number per cell) and conducted a global analysis of protein PTM in *Arabidopsis*. To this end it was essential to develop a method that allows deep sampling of the plant proteome in a reasonable time frame. It was clear that this sampling would have to begin with comprehensive extraction of tissue proteins and further entail multi-step fractionation of the complex extract. We settled on and optimized 4% SDS protein extraction and GeLC-MS combining SDS–PAGE protein separation and reverse-phase LC peptide separation on-line with electrospray ionization MS (see Supplementary methods and data and Supplemental Figure 1 for full method and optimization details).

Despite technological advances and deep sampling of the proteome, a long-standing caveat in proteomics remains proteomics "dark matter" (Skinner and Kelleher, 2015), meaning an abundance of high-quality MS/MS (MS2) spectra that do not result in a peptide spectral match (PSM). Many of these MS2 spectra are derived from peptides bearing PTMs; however, classic search algorithms necessitate PTM predefinition, limiting identification to a handful of potential PTMs. Recent years have seen the advent of "open search" algorithms (Chick et al., 2015; Kong et al., 2017; Bagwan et al., 2018; Chi et al., 2018) that allow unrestricted precursor mass shifts in PSMs and thus have the potential to identify the vast array of biologically occurring modifications on a proteome-wide scale. In this study, we performed such a survey using the MSFragger (Kong et al., 2017) software suite in *Arabidopsis*.

Extensive coverage of the proteome makes large-scale protein co-expression analysis a potentially powerful strategy to determine functional relationships between proteins because it circumvents the limitations inherent to transcriptomics measurements described above (Kustatscher et al., 2019). We applied clustering algorithms to our datasets, which provide extensive coverage of the *Arabidopsis* proteome, to uncover tissue-specific and developmentally specific protein expression patterns. The approach was effective in pinpointing co-regulation of all components of protein complexes and developmentally timed signaling modules. More importantly, it also allowed inference of previously unknown functions of proteins, protein families, and entire signaling modules based on the same expression patterns. This included processes, such as tissue- and age-specific ribosome biogenesis, photosynthesis, ABA signaling, and NAC transcription factors in seed development and establishment of dormancy as well as senescence and abscission.

Ribosomal proteins (RPs) are commonly found in proteomics studies. The various sequential steps of ribosome biogenesis, including the RPs and ribosome biogenesis factors (RBFs) involved, are well described in yeast and humans (Henras et al., 2008, 2015). Mutations in numerous RPs and RBFs are known to cause severe developmental defects, so-called ribosomopathies in humans. This also holds true in *Arabidopsis*, in which a number of mutations in RBFs affect gametophyte development and embryogenesis (Byrne, 2009; Weis et al., 2015). Furthermore, *Arabidopsis* ribosomes are extensively heterogenic, with each individual RP being encoded by two to seven paralogs (Weis et al., 2015). This heterogeneity of ribosome species depends on developmental stage, tissue, and environmental stimuli, suggesting that the specific ribosome constituency may play a regulatory role in these processes.

Early in the plant life cycle, cotyledons of young seedlings are characterized by light-induced chloroplast biogenesis (Waters and Langdale, 2009). Photomorphogenesis includes

tetrapyrrole and chlorophyll biosynthesis to establish photosystems along with carotenoid synthesis as an accessory pigment and reactive oxygen species (ROS) scavenger. Once photoautotrophic growth is established, protein biosynthesis is ramped up, hallmarked by the increased abundance of RPs and proteins involved in translation and folding. Concomitantly, nuclear encoded proteins synthesized in the cytosol are imported into the chloroplast. Finally, mature chloroplasts with their established structures proliferate by division to accommodate cell expansion and division in the growing leaves.

At the end of the life cycle, the plant undergoes senescence, which is a coordinated process with several stages and developmental check points (Bleecker and Patterson, 1997; Rogers and Munne-Bosch, 2016). Early senescence syndrome involves reprogramming of gene expression (Breeze et al., 2011) and redox and ROS signaling. This is followed by ordered dismantling of the photosynthetic apparatus, leading to ROS production and involving ROS control and nutrient remobilization to other plant parts in the case of leaves and to the developing ovary in the case of floral petals. The final result is cell death, followed by abscission in some organs, such as floral petals.

The plant immune system is integrally linked to the activity of phytohormones. Salicylic acid (SA) and jasmonate (JA) are quintessentially associated with plant defense, the former constituting the backbone of resistance to biotrophic pathogens, the latter to necrotrophic pathogens as well as wounding (Pieterse et al., 2012). Mutual antagonism between SA and JA to prioritize one defense strategy over the other as needed is a long-standing paradigm in the field of plant immunity. However, research in the last decade has made it clear that JA also plays a role in resistance to biotrophs and pattern-triggered immunity (PTI), which is however not yet fully understood (Nickstadt et al., 2004; Hillmer et al., 2017; Mine et al., 2017). The transcription factor JASMONATE INSENSITIVE 1 (MYC2) and its homologs MYC3 and MYC4 are master regulators of JA activity in the response to wounding and insects (Schweizer et al., 2013). It has been shown that they induce the expression of JA biosynthesis as well as JA- (and JA-isoleucine [JA-Ile])-conjugating genes, such as JASMONATE RESPONSE 1 (JAR1) (Staswick and Tiryaki, 2004), and catabolic enzymes, such as JA oxidases JASMONATE-INDUCED OXYGENASE 2 (JOX2) and homologs JOX3 and 4 (Caarls et al., 2017; Smirnova et al., 2017), as well as cytochrome P450 oxidases CYP94B1, B3, and C1 (Kitaoka et al., 2011; Koo et al., 2011, 2014; Heitz et al., 2012) in response to wounding (Zhang et al., 2020). IAA-ALA RESISTANT3 (IAR3) deconjugates JA-Ile to JA (Davies et al., 1999; Woldemariam et al., 2012; Widemann et al., 2013). These enzymes together tightly control JA levels and activity. Their functional interactions also potentially play a role in PTI and may reconcile the well-known dampening of JA levels and suppression of JA signaling downstream of JA synthesis by SA, adding another feature to the picture of JA activity in PTI.

RESULTS

Deep Proteomics Method

We conducted discovery proteomics measurements of several *Arabidopsis thaliana* Col-0 tissues throughout the lifetime of the plant. These were roots, leaves, cauline leaves, stems, flowers, and siliques/seeds, as well as whole plant seedlings sampled as early as 7 days up to 93 days of age when the plant was in late senescence (Supplemental Figure 2 and Supplemental Methods and Data Tables 1 and 2). In addition, to validate the applicability of our experimental procedure to a direct comparative deep proteomics approach, we measured proteomes of PTI-elicited plants treated with the peptide flg22.

Plant tissue is more recalcitrant to proteomics analysis than other samples. The plant cell wall requires harsh disruption techniques. Plant tissue contains an abundance of secondary metabolites, oils, and waxes and, more significantly, in the case of green tissue, pigments as part of the light-harvesting complexes, which all interfere with LC-MS. Green tissue also contains the most abundant protein on earth, ribulose bisphosphate carboxylase (RuBisCo), leading to suppression of less prominent ion signals in the mass analyzer and severely hampering detection of less-abundant proteins.

SDS–PAGE protein separation before LC-MS (GeLC-MS) alleviated all of these issues (Supplemental Figure 3A): (1) it allowed the depletion of high amounts of SDS (4%) used for protein extraction. (2) Pigments and small molecules conglomerated in a green low-molecular-weight band below the protein front, effectively partitioning them from the proteins. (3) RuBisCo large and small subunits (RBCL and RBCS) migrated as two prominent bands, facilitating their separation from the rest of the proteome.

Proteins in five gel slices were in-gel digested with trypsin and individually injected into the LC-MS, neatly fractionating the proteome according to the molecular weight of its constituents (Supplemental Figure 3B). The most abundant plant proteins including RBCL and RBCS were separated into individual fractions in both leaves and roots, diminishing the suppressive effects of over abundant proteins on peptide and protein identification in single-shot LC-MS measurement of the entire proteome (Supplemental Figure 3C and D). This allowed the identification of between 5977 and 9524 protein groups per sample, each identified with at least one unique peptide at protein and peptide false discovery rate (FDR) thresholds of 1%. These protein groups will henceforth be referred to as proteins (Supplemental Table 1 and Supplemental Figure 3E).

Our method is based on in-gel protein fractionation, gel division, and measurement of the respective gel sections individually. Repeatability and reproducibility may be critical issues. Therefore, we not only optimized the gel fractionation procedure but took the utmost care in our laboratory to fractionate every sample identically. Supplemental Figure 4 shows gel fractionation of different samples by two operators and shows the high repeatability of the gel pattern in our hands. We also checked the repeatability of the quantitative MS results by replicating samples and comparing their measurements to those of biologically distinct samples. The proteome sample of 93-day-old siliques (FF93) was replicated and the measurements directly compared with those of 90-day-old siliques and 90-day-old cauline leaves (FF90 and JLF90). The intrasample variability was considerably lower than the observed intersample variability (Supplemental Figure 3F and 3G),

indicating that the repeatability of the entire procedure was high. In addition, we replicated another proteome sample in an unrelated study on TZF9 function by different sample handlers and again compared the quantitative measurements (Supplemental Figure 5). The Pearson correlation between the replicate samples was high (0.98) and higher than that when measurements for replicates one and two were compared with the measurements for another distinct sample (0.933 and 0.946, respectively). The sample types were highly similar; the same tissue was collected, the replicated samples treated with flg22 for 2 h, and the comparison sample was untreated. Together these results indicate that our method can discriminate even very similar proteomes and that in our hands the entire procedure is repeatable.

The *Arabidopsis* Proteome

In the entire study we identified and quantified 15 926 *A. thaliana* proteins in total, 15 845 of which were encoded in the nuclear genome (Supplemental Table 2). We measured changes in the protein abundance of more than 2000 proteins functioning in all avenues of PTI as well as photosynthesis and primary metabolism, giving a comprehensive picture of altered proteome architecture in basal immunity. For further details on the parameters of the entire dataset see the Supplemental Methods and Data Table 3.

The proteins identified in our study were concatenated with those identified in the other two recently published protein atlantes (Mergner et al., 2020; Zhang et al., 2019), to give a complete picture of the *Arabidopsis* proteome supported by mass spectrometric evidence (Figure 1A). In total, these were 20 282 proteins. We complemented the proteomics data with the RNA sequencing transcriptomics data from an extensive study of *Arabidopsis* tissue development that measured gene expression of 24 964 nuclear loci (Mergner et al., 2020). Our proteomics data present mass spectrometric evidence for cognate protein expression of 60% (and locally more) of the *Arabidopsis* nuclear genome and close to 70% or more of the transcriptome, including 365 proteins for which no transcripts were identified (Figure 1B and 1C). The combined set of identified proteins represents well over 70% coverage of the entire nuclear genome and locally more than 80% coverage of the measured transcriptome. Nuclear protein identifications were evenly distributed over all five chromosomes (Figure 1C).

We then asked what precluded more extensive coverage of the *Arabidopsis* proteome in our study, i.e., the missing proteome. We first looked at the potential impact of transcript abundance on the detection of cognate proteins and found that missing (not detected) proteins are evenly distributed over the range of transcript abundance with the exception of the most abundant transcripts for nearly all of which a cognate protein was detected (Figure 1D). This indicates that transcript abundance is not the primary factor impeding protein detection. Next we investigated if gene length in base pairs as a proxy for protein length may have an impact and found that indeed the distribution of missing proteins was shifted markedly toward smaller genes from the distribution of detected proteins (Figure 1E). This suggests that protein size is a factor limiting protein detection. This effect could be observed for several gene ontology (GO) categories that were overrepresented in the missing proteome most obvious for nuclear and mitochondrial proteins (Figure 1F and Supplemental Figure 6). Then we examined how tissue-specific protein expression contributed to the cumulative expression of the entire proteome (Supplemental Figure 7). While every tissue contributed to the cumulative protein expression curve with a steep slope, it can also be seen that the curve converges on saturation as sample numbers increase. This was also the case for flg22-treated tissues plotted last, where one could expect expression of a host of immunity-specific proteins not detected in normally developing tissue (Supplemental Figure 7).

We quantified all 15 927 measured proteins in terms of protein copy number per cell in the entire sample set and in leaf tissue (LF) using the proteomics ruler approach (Wisniewski et al., 2014), which equates the total histone MS signal (total number of histone PSMs in our case) to the cellular DNA mass, allowing the conversion of PSMs to mass units and calculation of the total cellular protein mass. Individual to total protein PSM ratios can then be used to calculate individual protein copy numbers per cell.

The total cellular protein mass was calculated as 256.5 pg, in agreement with previous amounts from cell lines and tissues (Wisniewski et al., 2014). Protein copy numbers spanned a range of more than five orders of magnitude from just below 100 to 2.29e+07 copies per cell (Figure 1G, Supplemental Table 3). The most abundant protein was RBCL with 4.73e+07 cellular copies in leaves. The total copy number of all detected small subunits was 5.4e+07, so the ratio of large to small subunits was 0.876, close to a 1:1 ratio. GO analysis of the proteins in the four quartiles showed that nuclear proteins and regulators of transcription were very specifically among the least abundant proteins (1750 of 3970 first quartile proteins were annotated as nucleus). Membrane-spanning proteins and kinases were generally also less abundant, with 1108 of 3970 second quartile proteins being annotated as integral membrane proteins.

To address the potential for error in quantification of low abundant proteins using the protein quantification index "Total Spectral Count" (#PSMs), we investigated the effect of removing proteins with #PSMs < 5 from the proteomics ruler calculations of the protein copy numbers per cell. This effect was not pronounced, however, because nearly all histone proteins, which are the normalization "ruler," had #PSMs > 5. Furthermore, we performed the same absolute protein quantification calculations on the data from Mergner et al., where quantification was iBAQ based, i.e., based on peptide area under the curve measurements. The distribution of protein copy numbers per cell for all proteins shared between the two studies was highly similar, and the $\log_2$ copy numbers per cell of each individual protein showed a correlation (R^2) of nearly 0.7 and, perhaps more importantly, a linear regression slope close to 1 (0.83), indicating high proportionality between cellular copy numbers in the two studies (Supplemental Figure 8). Considering that the studies used different tissues and were not from the same laboratory, we conclude that the protein copy-number estimates that we calculated are reasonably good estimates of absolute protein amounts in both studies.

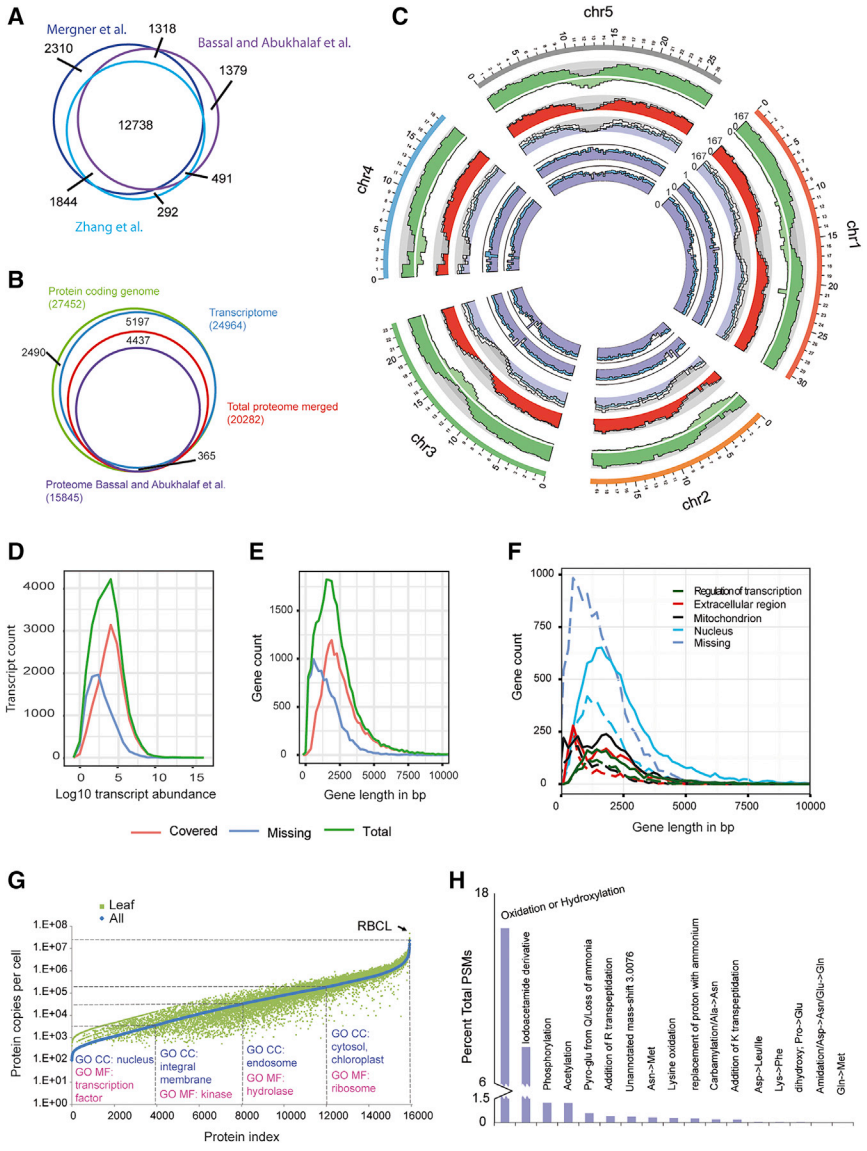

Figure 1. Deep Coverage of the *Arabidopsis thaliana* Proteome.

(A) Scaled VENN diagram comparing the three *Arabidopsis* tissue atlantes (Mergner et al., 2020; Zhang et al., 2019; and Bassal and Abukhalaf et al., this study).

(B) Scaled VENN diagram showing the coverage of protein coding genes by cognate transcripts and proteins from Mergner et al. (2020) (transcripts) the combined set of proteins derived from all three atlantes and this study (Bassal and Abukhalaf et al., this study).

(C) Mapping protein expression to the five *Arabidopsis* nuclear chromosomes (scale in megabases [Mb]). Tracks from outside to inside: number of protein coding genes per 500 kb; scale 0–167 (maximum) (dark green). Number of non-protein coding genes per 500 kb; scale 0–167 (light green). Number of transcripts per 500 kb; scale 0–167 (red); note number of protein coding genes per 500 kb as in outermost track is superimposed (white). Number of proteins per 500 kb; scale 0–167 (light purple). Number of proteins per 500 kb in all three studies, i.e., total proteome merged from **(B)** is superimposed (light blue) and number of protein coding genes per 500 kb as in outermost track is superimposed (white). Fraction of transcripts for which cognate proteins were detected; scale 0–1 (dark purple); fraction of total proteome merged is superimposed (dark blue). Fraction of protein coding genes for which cognate proteins were detected; scale 0–1 (dark purple); fraction of total proteome merged is superimposed (dark blue).

(D) Relationship between transcript abundance and detection of its cognate protein. Green, all protein coding transcripts; red, protein coding transcripts with a detected cognate protein; blue, protein coding transcripts without a detected cognate protein. Frequency polygon drawn with 20 bins.

(E) Relationship between protein coding gene size in bp and detection of its cognate protein. Green, all protein coding genes; red, protein coding genes with a detected cognate protein; blue, protein coding genes without a detected cognate protein. Frequency polygon drawn with bin size 190 bp.

(F) Size in bp of genes assigned to the gene ontology (GO) terms regulation of transcription, DNA templated (GO:0006355), extracellular region (GO:0005576), mitochondrion (GO:0005739), and nucleus (GO:0005634). Solid lines indicate all members of the GO term, dashed lines indicate members of the GO term not identified in the proteomics measurements, i.e., the missing proteome. Gene size of all proteins not identified in the proteomics measurements, i.e., the entire missing proteome, is also indicated. Frequency polygon drawn with 350 bins and bin size 190 bp.

(G) Copy numbers per cell of all identified proteins and leaf proteins as determined by the proteomics ruler method (Wisniewski et al., 2014). Quartiles are indicated by dashed lines. Significantly enriched GO annotations identified by DAVID are shown for the individual quartiles.

(H) Global survey of PTM in the *Arabidopsis thaliana* proteome. The relative abundance of PTMs comprising 0.1% or more of the total PSMs in at least one tissue type or biological scenario (flg22 treatment) are shown.

Protein PTM is an essential modulator of protein function. Therefore, we performed a proteome-wide survey of global PTM in *A. thaliana* with our deep proteomics dataset using the open search algorithm MSFragger (Kong et al., 2017). This led to the identification of more than 3.5 million PSMs from more than 11.6 million total acquired MS2 spectra. The most abundant PTMs comprising more than 0.1% of total PSMs in at least one tissue type or biological scenario are shown in Figure 1H (for full data see Supplemental Table 4). Next to predominantly experimentally induced PTMs (protein oxidation and carbamidomethylation of cysteine residues to reduce disulfide bonds), serine or threonine phosphorylation and N-terminal acetylation were the most abundant naturally occurring modifications affecting approximately 1.25% of total protein abundance. Addition of amino acids from transpeptidation, a non-translational mechanism for the formation of peptide bonds, was also detected. Furthermore, a number of amino acid substitutions in the protein primary structure were common.

Architecture of Tissue and Developmental Proteomes

We utilized our extensive MS data collection as a resource to investigate individual tissue proteomes during the *Arabidopsis* life cycle and co-regulation of protein abundance between them (Supplemental Table 5). First we grouped all of the data specifically by tissue, also merging rosette and cauline leaves, and qualitatively compared the tissue proteomes, which each comprised around 10 000 proteins (Supplemental Table 6). Around 6500 proteins (by far the largest set), were ubiquitous to all tissues, whereas 500 to 600 proteins were unique to each tissue with the exception of leaves, which showed nearly 1000 unique proteins, perhaps as a consequence of the larger number of aggregated leaf samples (Figure 2A). Also, around 1000 proteins were absent in roots but present in all other tissues, reflecting their below ground nature.

The large volume of data made principal-component analysis (PCA) an attractive method to reduce its dimensionality and explore the relationships of the sampled proteomes. The first two principal components accounted for nearly 50% of the total variance, indicating that the linear projection in this two-dimensional subspace reflects the predominant data structure (Figure 2B). The individual tissue proteomes were clearly separated with the exception of flowers and the inflorescence stem at the same points in development (66 and 73 days). More interestingly, a developmental component was also visible in all sampled tissues, reflecting proteome remodeling during aging (increasing sample age bottom right to top left; arrow). Hierarchical cluster analysis corroborated the PCA results (Supplemental Figure 9).

To investigate the dynamics of proteome structure and protein co-expression in tissue development in detail and thereby extrapolate protein function in previously undisclosed contexts, a noise-robust soft partitioning technique that does not assign a feature exclusively to a single group, called fuzzy c-means clustering, was applied (Futschik and Carlisle, 2005). The procedure produced 16 clusters, 7 of which (clusters numbered 3, 4, 7, 8, 10, 11, and 13) had biologically meaningful changes in protein abundance with a permutation-based FDR of less than 1%.

Root Proteome

The largest set of 577 proteins assigned to a cluster were root specific and not abundant or present in any other tissues at any of the sampled developmental stages (cluster 3, Figure 2C, Supplemental Table 7). GO analysis of these proteins indicated that many of them were involved in processes related to the extracellular region, metal binding, and oxidation and reduction. We previously described the expression of these proteins in the context of phosphate metabolism (Hoehenwarter et al., 2016). We compared our results with measurements of the root proteome from soil-grown 22-day-old roots, 7-day-old root tips, and 7-day-old root upper zones as described by Mergner et al. (2020), and to the results of another exhaustive study of the root proteome by Lan et al. (2012) (Figure 2C, center panel). We found that around 90% and 80% of the total root proteins we detected were also identified in the other two studies, respectively. The intersection between all three studies constituted 7028 proteins and allows us to define the core set of proteins most abundant in the root, the root core proteome (see Supplemental Table 8).

Seed Proteome

Cluster 7 (Figure 2D) contains proteins whose abundance increased specifically in seeds. As expected, many of these were the more abundant seed storage proteins, such as oleosins, albumins, cruciferins, and enzymes of sugar and fatty acid metabolism. However, many of the core transcription factor, phosphatase, and chromatin modifier modules that regulate seed development were also detected and quantified (Supplemental Table 9 and Figure 2D). The PP2C POL directs *WUS/WOX5* gene expression and is essential for meristem establishment and stem cell maintenance in the early embryo together with PLL1 (Song et al., 2008). Similarly, the AIL transcription factor BBM and HDG1 act antagonistically to balance stem cell proliferation and differentiation (Horstman et al., 2015), and AN3 establishes cotyledon identity upstream of PLETHORA1 (Kanei et al., 2012). The ABA signaling proteins, which are known to play a major role in seed development, were underrepresented in cluster 7 mainly because they either did not accumulate exclusively in seeds or did not accumulate in both of the measured stages (developing green and ripe brown siliques), but their abundance could be easily reconstituted from the data. LEC1, the master inducer of seed development was highly abundant in the earlier stage together with AREB3 and EEL, two ABA-responsive bZIP transcription factors that govern early seed maturation (Agarwal et al., 2011). The ratio of the bZIP transcription factor ABI5 to AFP1, a repressor of ABA signaling, both detected exclusively in mature to post-mature seeds, was greater than 1, which indicates high ABA levels and induction and possible maintenance of seed dormancy in the brown siliques sample. Concomitantly the DOG1 protein and the RDO5 PP2C, which are essential for seed dormancy (dormancy is completely abolished in the *dog1* knockout mutant also in the presence of ABA [Nee et al., 2017]), were abundant in the post-mature seed proteome. A number of other PP2C proteins also accumulated to high levels specifically in siliques, particularly in brown siliques. The same was true for several members of a clade of NAC transcription factors also hitherto not known to play a role in seed development, indicating potential functions for them in seed development and establishment of dormancy.

Ribosomal Proteins in Development

The abundance of the 315 proteins in cluster 4 strongly increased or was exclusively measured in young roots, young stems, and early flowers/floral buds. The abundance decreased in the latter two tissues as development progressed (Figure 2E). More than half of these proteins were localized in the nucleus, and a substantial number of them pertained to nucleolar processes and ribosome biogenesis, with WD40 proteins, which contain the WD40 repeat molecular interaction domain, being highly significantly enriched (Supplemental Table 10).

One of these was LEUNIG (LUG), a transcriptional co-repressor and master regulator of flower development that directly modulates antagonistic A and C class gene expression in the inner and outer whorls (Grigorova et al., 2011). TAIR10 annotated six WD40 proteins as DWD components of CUL4 RING E3

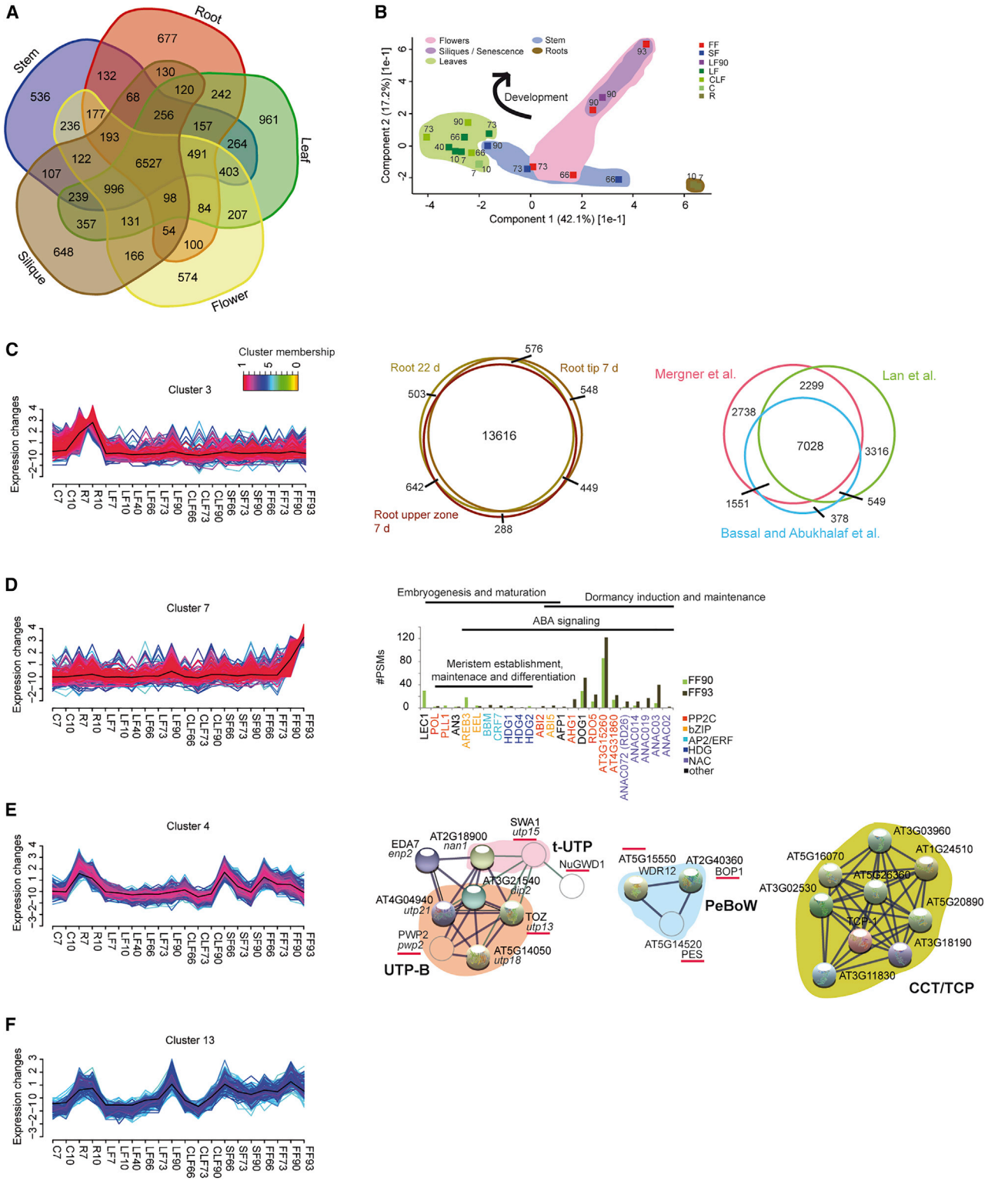

Figure 2. Tissue and Development-Specific Dynamic Architecture of the *Arabidopsis* Proteome.

(A) Qualitative comparison of *Arabidopsis* tissue proteomes. All measurements of a tissue regardless of plant age were aggregated (leaves and cauline leaves were aggregated as well).

(B) Principal-component analysis (PCA) of the deep proteomics measurements of sampled tissues. Numbers indicate sample, i.e., plant age in days. Tissues are color coded. Purple indicates late-flowering stages, i.e., siliques and leaves undergoing senescence.

(legend continued on next page)

ubiquitin ligases (Supplemental Table 10), but closer inspection revealed that AT3G56990 (EDA7) and AT4G04940 actually lacked the canonical DWD motif (Supplemental material and data), while the others belonged to the A clade of *Arabidopsis* DWD proteins (Lee et al., 2008). Among them was DWA2, a negative regulator of ABA signaling that targets ABI5 for degradation (Lee et al., 2010).

We investigated potential interactions among the 18 WD40 proteins in cluster 4 using the STRING database set to produce essentially only true positive binary physical interactions. Five of the six components of the UTP-B complex, a sub-complex of the SSU processome/90S pre-ribososme, were found to interact based on experimental evidence from yeast and humans (Gavin et al., 2002, 2006; Krogan et al., 2006; Wan et al., 2015), showing tissue- and development-specific expression of this entire protein complex (Figure 2E, Supplemental Figure 10 and Supplemental Table 10 for raw abundance values). The complex interacted with EDA7, the homolog of enp2 (Soltanieh et al., 2014), a putative RBF that is not known in *Arabidopsis*. NuGWD1 a sugar-inducible WD40 protein was reported to interact with SLOW WALKER 1 (SWA1), which is a component of the t-UTP sub-complex of the SSU processome and which was also shown to interact with several UTP-B members by coimmunoprecipitation MS in *Arabidopsis* (Ishida et al., 2016). SWA1 is not a WD40 protein, but the pattern of its abundance was very similar to the protein expression pattern of the cluster 4 proteins (Supplemental Table 10 for raw abundance values). Another WD40 protein-containing complex, all of whose components were measured and showed the same expression pattern, elevated abundance in roots, young shoots, and early flowers/floral buds, was the PeBoW complex, which is essential for pre-rRNA processing (Cho et al., 2013; Ahn et al., 2016). In addition, extensive physical interaction between a large number of RPs and other ribosome-associated proteins with this expression pattern became evident when interactions between all 315 cluster 4 proteins was assayed (Supplemental Figure 10). However, the expression patterns of the cluster 4 RBF protein complexes were significantly more conserved than those of the RPs (Supplemental Figure 11).

Molecular chaperones were also highly significantly enriched among the cluster 4 proteins. Nine of these 21 proteins putatively interact physically based on X-ray crystallography and tandem affinity purification studies in yeast and humans (Dekker et al., 2011; Hauri et al., 2016). All of these TCP-1/cpn60 proteins are homologs of the yeast and human cytosolic chaperonin CCT proteins, suggesting that they constitute the little-described CCT complex in *Arabidopsis* and that its abundance is tissue- and developmentally specific (Figure 2E and Supplemental Table 10 for raw abundance values).

Vesicle Trafficking and Transport

A set of 153 proteins were abundant in roots, showed increasing abundance in leaves during aging, peaking during senescence, and also showed increased abundance in the young inflorescence stem and flowers (cluster 13, Figure 2F and Supplemental Table 11). These proteins were largely related to vesicle trafficking, Golgi apparatus, and membrane transport. They contained numerous exocyst complex members, SNAREs, and cytoskeletal proteins, such as actin. Vesicle trafficking and cytoskeletal remodeling and organization are central processes in tip growing cells, such as the well studied root hairs (Rounds and Bezanilla, 2013), but are also prevalent in fast growing tissues, such as the emerging inflorescence stem and flowers (Chen et al., 2009). On the other hand, autophagy, a process that also involves the formation of lytic compartments and vesicle trafficking for the degradation of cytoplasmic material, is known to play an important role in senescence in leaves and other tissues (Wojciechowska et al., 2018).

The Proteome in Establishment and Maintenance of Photosynthesis

Clusters 11 and 8 (Supplemental Tables 12 and 13, respectively) were almost exclusively comprised of proteins annotated as chloroplast localized (297 of 326 nuclear plus 18 plastid encoded and 223 of 264 nuclear plus 20 plastid encoded, respectively) and annotated as essential to photosynthesis by DAVID GO. Proteins were absent in roots and mature brown siliques and predominant in green tissues, primarily in leaves and cauline leaves. The abundance of cluster 11 proteins peaked in cotyledons of 7- and 10-day-old seedlings and young cauline leaves, and declined in these tissues over the course of aging, whereas cluster 8 proteins were consistently abundant in rosette leaves throughout the plant lifecycle, with a slight maximum at 40 days, and declined during senescence (Figure 3A and 3B).

The proteins in cluster 11 primarily function in chloroplast biogenesis and the establishment of the functional photosynthetic machinery. A number of central players in these molecular events were identified, including HEMA1 and GUN5 (as well as

(C) Fuzzy C Means (FCM) cluster 3 showing proteins exclusively abundant in roots. Center panel: total root proteome as reported by Mergner et al. (2020) Right panel: qualitative comparison of root proteomes reported by (Mergner et al., 2020; Lan et al., 2012; and Bassal and Abukhalaf et al., this study). FCM core clusters were extracted wherein all clustered proteins have membership α values exceeding a threshold of 0.5, indicating that cluster members all have similarity to the cluster centroid greater than 0.5 (Futschik and Carlisle, 2005).
(D) FCM cluster 7 showing proteins increasing in abundance during seed development and exclusively present in seeds or siliques. Right panel: protein abundance of kinases and transcription factors (protein quantification index [PQI] given is raw #PSMs) in the respective samples.
(E) FCM cluster 4. Right panel: physical protein interaction networks produced with the STRING database based on homology to proteins from yeast and human studies. Solid spheres in the UTP-B, t-UTP, and PeBoW networks are proteins designated as DWD40 by DAVID gene ontology analysis and part of the respective STRING input dataset (WD40/YVTN repeat-like-containing domain list Supplemental Table 10). Unfilled spheres are not part of the WD40 input set but are also members of cluster 4. Thin black edges indicate bona fide physical interactions identified in humans (Wan et al., 2015). Green edges indicate bona fide physical interactions identified in *Arabidopsis* (Ishida et al., 2016). Red underlines indicate that deletion of the gene results in a developmental phenotype. Yeast homologs of *Arabidopsis* genes are given in italics.
(F) FCM cluster 13.

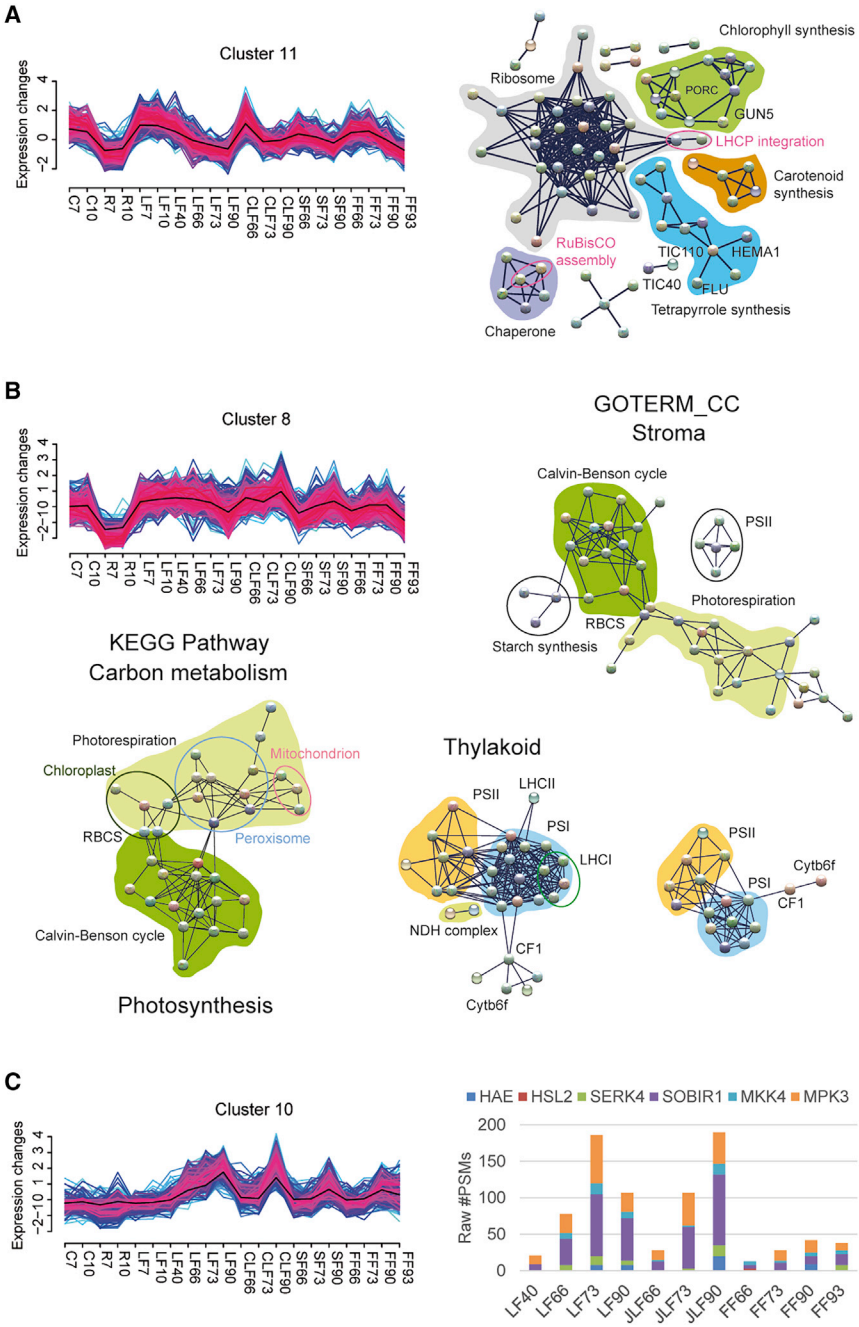

Figure 3. Proteome Remodeling in the Establishment and Maintenance of Photosynthesis, Degradation of Photosynthetic Apparatus, and Leaf Senescence.

(A) FCM cluster 11. Right panel: physical/functional protein interaction networks generated with the STRING database using all proteins assigned to the GOTERM category Chloroplast (Supplemental Table 12) as the input set. Various biochemical pathways involved in pigment- and photosynthesis-related protein synthesis and chloroplast biogenesis are color coded and indicated.

(B) FCM cluster 8. Right panel: physical/functional protein interaction networks generated with the STRING database using all proteins assigned to the GOTERM categories Stroma, Thylakoid, Carbon metabolism (C Metabolism), and Photosynthesis as input sets (Supplemental Table 13). Light-independent reactions are highlighted in green (Calvin-Benson cycle, dark; photorespiration, light) and light-dependent reactions in orange (photosystem II [PSII]) and blue (photosystem I [PSI]).

(C) FCM cluster 10. Right panel: cumulative abundance (protein quantification index [PQI] given is raw #PSMs) of core abscission signaling module proteins in leaves, cauline leaves, flowers, and siliques.

Toc/Tic complex including TOC33, which is known to be most strongly expressed in young seedlings, were cluster members (Waters and Langdale, 2009). The two proteins forming the inner division ring mediating chloroplast division, FtsZ1 and FtsZ2, were also cluster members (Waters and Langdale, 2009). DAVID GO (Huang da et al., 2009) mapped the cluster proteins to several plastid structures thereby giving a possible inkling of their localization within the chloroplast.

Cluster 8 mostly contained proteins prevalent in mature chloroplasts that are directly related to photosynthesis. Cluster members constituted extensive parts of both the light-dependent and -independent reactions. Regarding the former, most components of the oxygen-evolving photosystem II (PSII) and photosystem I (PSI), providing the final strong reducing potential, were identified, many of them being close interactors (Figure 3B). Components of the electron-transferring $Cytb_6f$ complex and the thylakoid ATP synthase CF_1 were also present. Regarding carbon fixation, nearly all components of the Calvin–Benson cycle and many of the proteins involved in photorespiration were mapped as functional interaction partners (Figure 3B). Furthermore, functional interaction mapping could resolve organelle specificity of the individual reactions in photorespiration. Interaction networks produced from the GO category stroma and carbon metabolism protein set, and from the GO category thylakoid and

GUN4) (Liu et al., 2017), which also represent hubs in STRING-generated networks of cluster member proteins interacting in tetrapyrrole and chlorophyll synthesis, respectively (Figure 3A, complete annotated network Supplemental Figure 12). Other cluster proteins were interaction partners in carotenoid synthesis. Around 30 cluster proteins were classified as RPs or related to translation by DAVID GO, which was reflected by a highly connected interaction network composed of chloroplast-specific RPs, ribosome-associated proteins, or RBFs, the gene knockouts of many of which have embryo-lethal phenotypes. CPN60 and CPN10 class molecular chaperones formed another cluster of interactors. Protein import from the cytosol is essential to chloroplast biogenesis, and constituents of the

photosynthesis protein set, were specific and showed extensive overlap, attesting to the quality of protein extraction from the chloroplast compartments (full annotated networks Supplemental Figures 13–16).

The Proteome in Senescence

Cluster 10 contained 241 proteins whose abundance increased substantially during the course of the plant life cycle and peaked in the latest developmental stage, i.e., during leaf and flower senescence and fruit ripening, predominantly in rosette leaves, but also in cauline leaves, stems, and flowers (Supplemental Table 14). These proteins were not abundant in young tissues (Figure 3C).

Senescence is a controlled developmental process that entails disassembly of the photosynthetic apparatus for the pupose of nutrient remobilization in leaves and resource allocation to fruit ripening in flower petals (Bleecker and Patterson, 1997). Conversely, numerous proteins involved in chlorophyll and carotenoid degradation were found, including pheophorbide, an oxidase that is the key enzyme in the formation of primary fluorescent chlorophyll catabolites (FCCs). It has been shown that nonfluorescent dioxobilin-type chlorophyll catabolites (NDCCs) represent the major end-products of chlorophyll catabolism as opposed to NCCs and that the cytochrome P450 monooxygenase CYP89A9 is responsible for their accumulation (Christ et al., 2013). This protein was also a cluster member as well as 13 other CYPs. Twelve of the 14 total CYPs belonged to the CYP71 clan, suggesting a broader role for these proteins beyond CYP89A9.

During senescence large amounts of ROS are produced, which must be controlled so as not to lead to tissue damage and premature cell death (Rogers and Munne-Bosch, 2016). Many cluster proteins were found to be involved in oxidative-reductive processes and ROS scavenging, including the centrally important cytosolic ascorbate peroxidase APX6. More interestingly, a significant group of cluster proteins were kinases. Six of these were cysteine-rich receptor-like kinases (CRKs) (CRK7, CRK8, CRK10, CRK14, CRK21, and CRK41), which have two extracellular DUF26 domains that each contains four conserved cysteine residues. The programmed loss of redox control leads to ROS accumulation and ultimately cell death at the later stages of senescence, and ROS may also play an important role in signaling, mediating genetic reprogramming during senescence (Breeze et al., 2011); the mechanisms of ROS in signaling, however, are largely unexplored. The CRK cysteine thiol groups are likely sensitive to the redox state, potentially implicating these proteins as ROS sensors and ROS signaling initiators in senescence.

Abscission of floral organs after fertilization is another developmental process that occurs late in the *Arabidopsis* life cycle. Most of the proteins of the canonical abscission signaling module (Meng et al., 2016), including the receptor-like protein kinases HAESA (HAE), HAESA-like 2 (HSL2), and EVERSHED (EVR/SOBIR1), the co-receptor SOMATIC EMBRYOGENESIS RECEPTOR-LIKE KINASE 4 (SERK4), and MKK4 and MPK3, the mitogen-associated protein kinase (MAPK) cascade downstream of the HAE receptor complex, were cluster members. The proteins accumulated in flowers and later in siliques as development progressed (Figure 3 C, right panel). Interestingly, their abundance also increased in leaves and cauline leaves, although leaf abscission is not developmentally timed, possibly suggesting an unknown function of this abscission signaling module.

Proteome Remodeling in Steady-State PTI

In addition to tissue proteomes and their alteration over the course of development, we were interested in assaying more rapid changes in proteome architecture such as those determined by steady-state shifts from ordinary growth to immunity. Seven- and 10-day-old seedlings grown in liquid culture were treated with a final concentration of 1 μM flg22 in the medium for 16 h. Flg22 is the 22-amino acid N-terminal epitope of flagellin and elicits PTI downstream of the leucine-rich repeat receptor-like kinase (LRR-RLK) FLAGELLIN-SENSITIVE 2 (FLS2). Deep proteomics measurement of the untreated and treated samples identified 8344 proteins in all (Supplemental Table 15). Hierarchical cluster analysis showed that the abundance of 1774 proteins increased, whereas the abundance of 915 decreased in both samples as a result of flg22 exposure (Supplemental Table 16).

These proteins were categorized by mapping them to a self-constructed model of PTI using MapMan software (see the Supplemental data for details, Supplemental Table 17, Supplemental Figure 17). The result was a comprehensive picture of proteome remodeling in PTI showing extensive changes in protein abundance in most of the major perception, signaling, and response pathways. Dynamics of the flg22 receptor complex, including decreased abundance of FLS2 as a result of internalization and degradation (Robatzek et al., 2006), and a host of other RLKs were quantified. Vesicle trafficking and transport proteins, including exocyst and SNARE complex members, increased in abundance along with proteins involved in the early respiratory burst, primarily RESPIRATORY BURST OXIDASE HOMOLOGUE D (RBOHD). All of the components of both MAPK signaling cascades central to plant immunity, MKK4/5-MPK3/6/11 and MKK2-MPK4 (Bigeard et al., 2015), were measured and also showed a slight increase in abundance. The same goes for the calcium-dependent protein kinases (CDPKs) integral to PTI signaling, CPKs 4, 5, and 6 (Boudsocq et al., 2010), as well as a host of other CDPKs, calmodulin (CAM) and CAM binding proteins, and calcineurin (Supplemental Table 18). Interestingly several proteins showing changes in abundance upon PAMP stimulus were mapped to other avenues of plant immunity, such as effector-triggered immunity, programmed cell death, and systemic acquired resistance (SAR).

We investigated proteome plasticity in more detail beginning with the category hormone signaling and branching out from it to produce a proteomics model of phytohormone activity in PTI (Figure 4, Supplemental Table 19). The deep proteomics results were complemented by measurements of the plant hormones themselves, amino acids, and secondary metabolites after 16 h of flg22 treatment. Furthermore, we undertook a retention time scheduled, parallel reaction monitoring (PRM)-based targeted proteomics study that

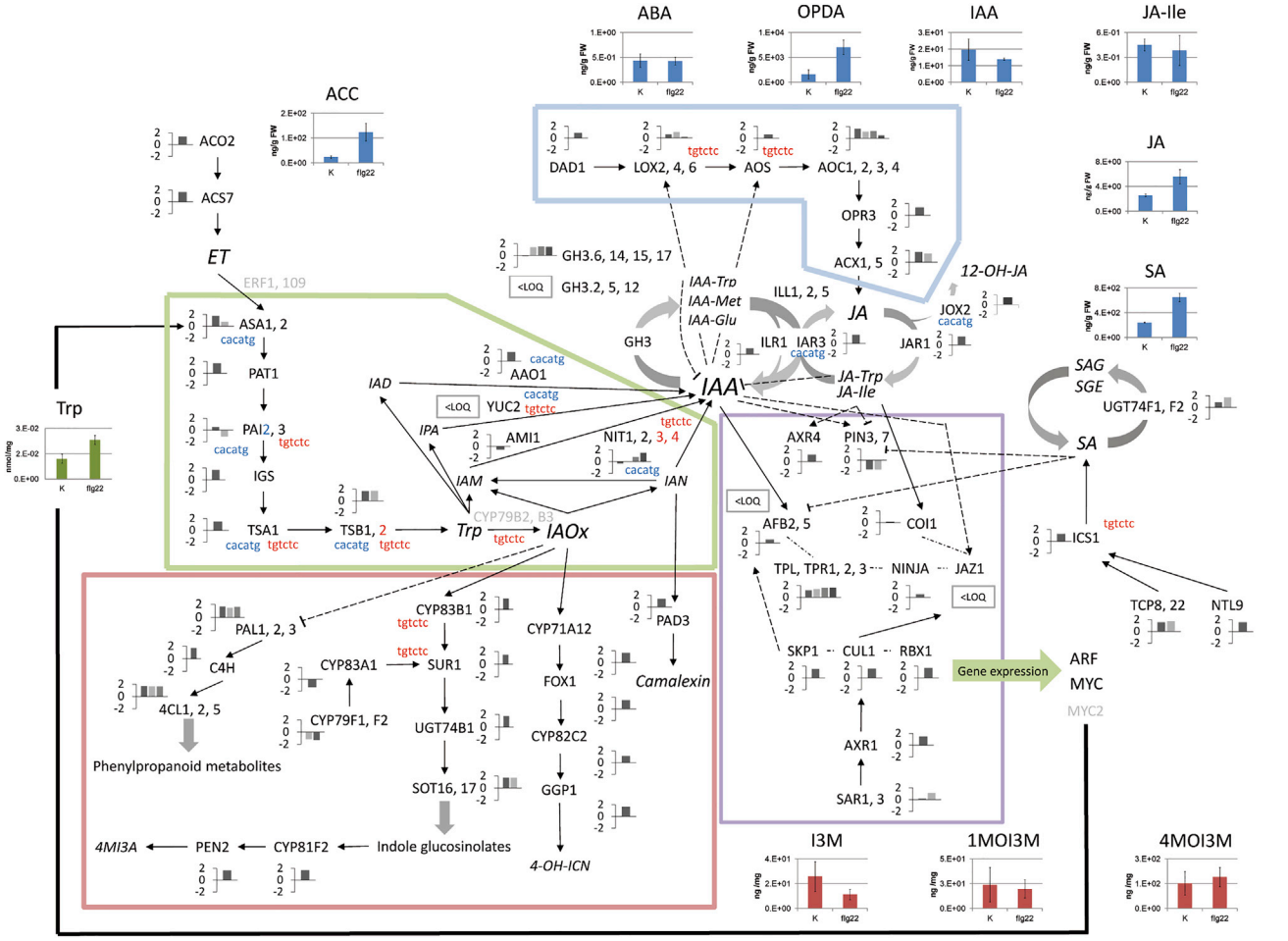

Figure 4. Proteomics Model of Phytohormone Activity in PTI.

The figure shows the proteins quantified in the jasmonate (blue), tryptophan and IAA (green), and secondary defense compounds/indolic glucosinolate (red) biosynthesis pathways, as well as the IAA and JA signaling pathways (purple). Note that all or nearly all components of these biochemical pathways were measured and quantified in the deep proteomics study. Proteins pertaining to ET and SA synthesis, as well as reversible hormone conjugation (GH3s) and modification, are also shown. Proteins with names in black were measured; bar charts next to protein names indicate relative changes in abundance after flg22 treatment; values are the sum of *Z* score-transformed raw #PSMs in flg22-treated samples. Proteins in gray were not detected. Red nucleotide sequence indicates an ARF1 binding site in the cognate gene promoter region, and blue a MYC2 binding site. Solid arrows indicate direct functional interaction or immediately neighboring steps in biochemical pathways. Dashed arrows indicate more distal interactions. Phytohormone, tryptophan, and indole glucosinolate abundances 16 h after flg22 treatment are also shown.

allowed accurate quantification and inference of statistical significance of fold changes of 52 model proteins in three sample pools of 10-day-old *Arabidopsis* seedlings, again following 16 h of flg22 treatment (Figure 5, Supplemental Table 20). The PRM-based estimates of protein abundance fold changes were in full agreement with the deep proteomics quantification, highlighting the latter's accuracy and the power of the deep proteomics strategy in general.

The abundance of 43 proteins playing roles in photosynthesis decreased slightly after 16 h of exposure to flg22 (Supplemental Table 21). Fifteen of these were assigned to the photosynthesis light reaction and six of these in turn to PSII by MapMan software (MapMan bins PS.lightreaction and PS.lightreaction.photosystem II.LHC-II, respectively, Supplemental Table 21). Both bin assignments were statistically significant (Benjamini-Hochberg corrected $p < 0.01$) indicating that these categories were enriched among the 43 proteins. Other proteins were assigned to the carbon reactions, more specifically the Calvin-Benson cycle (Supplemental Table 21). The relatively small decrease in abundance of a set of these proteins was corroborated by small yet significant fold changes (maximum decrease -0.6 $\log_2$ fold change) in the PRM study (Supplemental Figure 18 and Supplemental Table 20). These results suggest that photosynthesis is inhibited upon PAMP perception and thus in PTI.

The abundance of 93 proteins playing roles in plant primary metabolism, especially carbohydrate metabolism, increased upon exposure to flg22 (Supplemental Table 21). Twenty-two were categorized as pertaining to glycolysis (MapMan bin glycolysis), 19 to the TCA cycle (MapMan bins TCA/org. transformation.TCA and TCA/org. transformation.other organic acid transformations), and 6 to major CHO metabolism

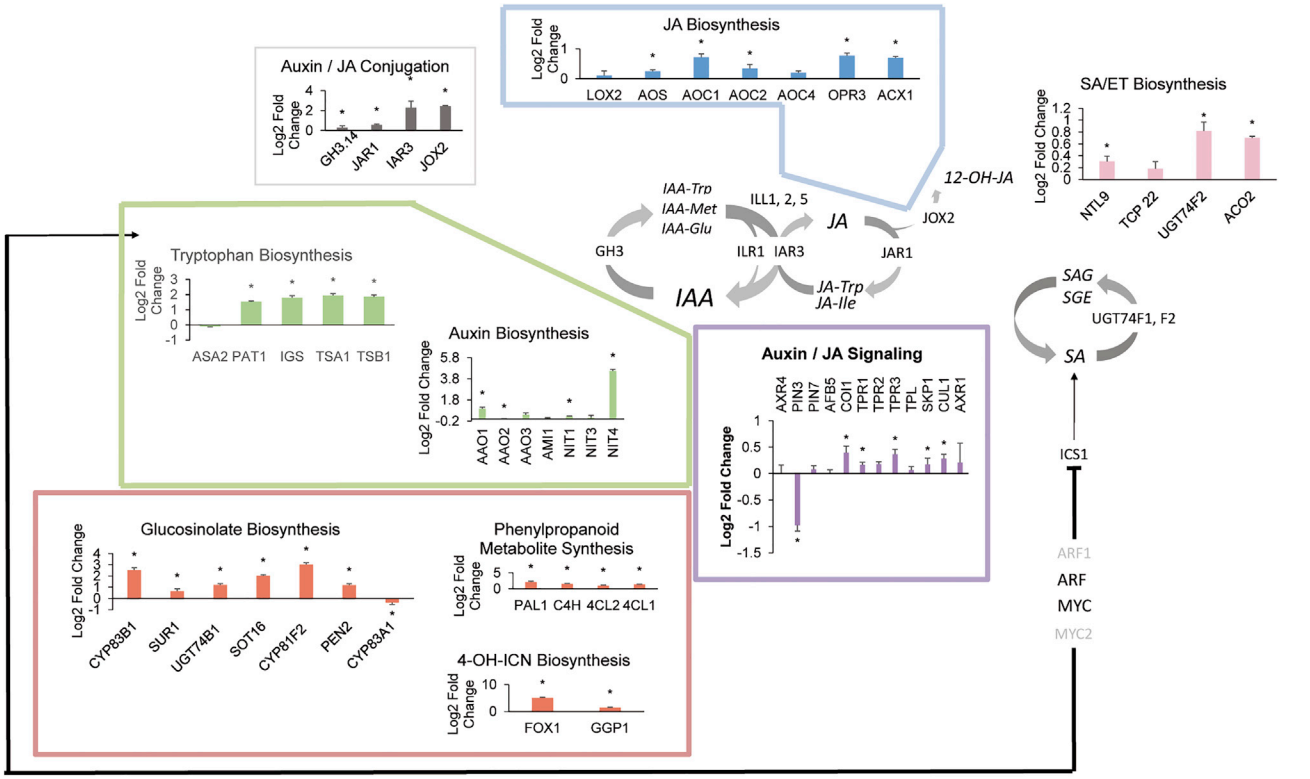

Figure 5. Targeted PRM-Based Quantification of Representative Proteins.
Framework is analogous to that in Figure 4. Bars represent log2 fold changes of protein abundance after 16 h of flg22 exposure (1 μM concentration in medium) estimated by area under the curve label-free protein quantification index (PQI) of the six most intense product ions from MS2 spectra of targeted proteotypic peptides. Bars represent median PQI of all quantified proteotypic peptides for a given protein in nine measurements (three biological replicates each measured three times). Standard error is indicated. Star indicates significance at $\alpha = 0.05$ if the fold change in abundance of at least one of the quantified peptides was significant in a permutation-based FDR-corrected two-sample *t*-test.

(MapMan bin major CHO metabolism.degradation.starch), among others by MapMan software. Increases in abundance were more pronounced than the downregulation of photosynthesis-related proteins, and $\log_2$ fold changes up to 1.6 were quantified and significant in the PRM study (Supplemental Figure 18 and Supplemental Table 20).

Jasmonate Conjugation and Catabolism in PTI

Sixteen hours of flg22 exposure led to an increase in the abundance of SA synthesis pathway proteins, primarily ISOCHORISMATE SYNTHESIS 1 (ICS1), the upstream transcription factors TEOSINTE BRANCHED1/CYCLOIDEA/PCF 8 and 22 (TCP8, TCP22) (Wang et al., 2015) and NTM1-Like 9 (NTL9) (Zheng et al., 2015), and free SA levels (nearly three-fold increase).

The levels of JA, and JA-isoleucine (JA-Ile), its bioactive conjugate, were both low; although levels of the former increased around two-fold, the levels of the latter showed no significant change and absolute levels of both were in the range of a few ng/g fresh weight (FW). Concurrently, (+)-12-oxo-phytodienoic acid (OPDA) levels increased from 1.6 to 7 μg/g FW, so the levels of OPDA were initially high and increased more than four-fold after flg22 treatment. OPDA is a primary JA precursor synthesized from allene oxides by ALLENE OXIDE CYCLASE 1 to 4 (AOC1 to 4). ACC, the ethylene (ET) precursor and a proxy for ET abundance, increased by more than five-fold.

The deep proteomics measurements showed elevated protein amounts of all components of the JA biosynthesis pathway, corroborated as significant in the PRM study. Moreover the core JA receptor complex/signaling proteins CORONATINE INSENSITIVE 1 (COI1), TOPLESS RELATED PROTEINS 1 to 3 (TPR1 to 3), and S PHASE KINASE-ASSOCIATED PROTEIN 1 (SKP1) and CULLIN 1 (CUL1) proteins, members of the E3 ubiquitin ligase SCF complex that are also components of the auxin and gibberellic acid (GA) signaling pathways, all significantly increased in abundance, albeit slightly. The abundances of a large number of GRETCHEN HAGEN (GH) enzymes, the amidohydrolase IAR3, and JOX2 also increased after exposure to the PAMP, the latter two significantly by around five-fold. These enzymes are all involved in conjugating or deconjugating phytohormones, specifically JA and auxin (IAA), to amino acids or small molecules or hydroxylating them (JOX2), thereby modulating their sub-cellular location and/or rendering them active or inactive.

Auxin/IAA Homeostasis in PTI

The detection of numerous GH proteins known to conjugate auxin/IAA (GH3.2, GH3.5/WES1, and GH3.17/VAS2) prompted

us to investigate the role of this phytohormone in PTI. The levels of GH3.14, GH3.15, and GH3.17 increased upon flg22 exposure, the first significantly, by 1.2-fold. GH3.15 (AT5G13370) function in conjugating the IAA precursor IBA has just recently been elucidated (Sherp et al., 2018). GH3.14 (AT5G13360), the neighboring gene, does not show any significant sequence homology to GH3.15, indicating a potentially different uncharacterized function in PTI.

Auxin/IAA is synthesized by tryptophan-dependent and -independent pathways (Mano and Nemoto, 2012; Kasahara, 2016). Both deep and targeted proteomics results showed significant substantial increases in the abundance of all proteins in the tryptophan biosynthesis pathway, and tryptophan levels also increased by almost two-fold after 16 h of PAMP treatment. Tryptophan channels into a host of defense-related secondary metabolite synthesis pathways, particularly synthesis of indole glucosinolates (IGs); the protein abundances of IG synthesis enzymes all increased highly (two-fold or more) and significantly. Levels of the IGs themselves, indol-3-ylmethylglucosinolate (I3M), 1-methoxy-indol-3-ylmethylglucosinolate (1MOI3M), and 4-methoxy-indol-3-ylmethylglucosinolate (4MOI3M), did not change significantly. Presumably they were hydrolyzed by the mirosinase PENETRATION 2 (PEN2), whose abundance increased by 2.3-fold in response to flg22, along with CYP81F2, which showed an 8.2-fold change in abundance, to play a role in callose deposition (Clay et al., 2009).

Several proteins potentially involved in auxin/IAA synthesis pathways were identified. The abundance of ALDEHYDE OXIDASE 1 (AAO1) increased by nearly 2-fold and that of the NITRILASES 1 and 4, by 1.2- and 23-fold, respectively. Auxin/IAA levels, however, decreased slightly (0.75-fold) but significantly ($p = 0.051$, two-sample *t*-test equal variance, $n = 5$, $\alpha = 0.1$). AAO1 has recently been shown to play a role in converting the I3M downstream hydrolysis product, indole-3-carbaldehyde, to indole-3-carboxylic acid during abiotic stress response (Muller et al., 2019). *Pseudomonas syringae* pv. *tomato* DC3000 (*Pst* DC3000) infection induced a strong transcriptional response of the nitrilases NIT2, NIT3, and NIT4, which was corroborated by increased protein abundance in the case of NIT2. It was postulated that NIT2 is involved in IAA signaling in R gene-mediated resistance and defense against biotrophic pathogens (Choi du et al., 2016). The more than 20-fold increase in the abundance of NIT4 that we measured suggests an unknown function of this protein in basal resistance to biotrophic pathogens.

Although auxin/IAA levels did not change substantially even 16 h after PTI induction, the abundance of polar auxin transporters was markedly affected. In particular, the abundance of PIN-FORMED 3 (PIN3), a polar efflux carrier with well-documented functions in lateral root growth and tropism, decreased significantly by two-fold. A similar decrease was apparent in the deep proteomics results for PIN-FORMED 7 (PIN7), which is also known to affect lateral root growth. Both PIN3 and 7 have important roles in establishing local auxin concentration maxima (Jang et al., 2018). The abundance of AUXIN RESISTANT 4 (AXR4), an ER protein that is responsible specifically for the distribution and localization of the influx carrier AUXIN RESISTANT 1 (AUX1), was also elevated slightly (Dharmasiri et al., 2006). PIN3, PIN7, and AUX1 are the primary components of the polar auxin transport system, so our results indicate that active, cell-to-cell auxin transport is perturbed in steady-state PTI (Friml, 2003; Blilou et al., 2005).

Chronology of JA and IAA Activity in PTI

It has been documented that JA, IAA, and SA act in chronological order in the establishment of SAR, and that JA and IAA play earlier roles (Truman et al., 2010b). Therefore, we measured JA hormone levels and the transcript and protein levels (by qPCR and PRM, respectively) of JA biosynthesis enzymes (blue box Figure 5), JA/IAA conjugation and metabolism enzymes (gray box Figure 5), JA/IAA signaling components, and the IAA transporters PIN3 and PIN7 (purple box Figure 5) 1, 3, and 16 h after flg22 treatment. We also profiled the abundance of the proteins involved in the synthesis of secondary metabolites/defense compounds (boxed in orange in Figure 5) at these time points. In addition, as our data potentially suggested previously little explored roles of both JA and IAA in PTI, we performed measurements of these hormones and the transcripts of JA- and IAA-related genes in the *myc234* background at these time points as a complement (Figure 6, and see Supplemental Tables 22 and 23 for all values and significance). MYC2 is one of the most important transcription factors in JA signaling downstream of COI1, and the triple knockout exhibits essentially no functional redundancy (Schweizer et al., 2013).

In the wild-type JA and JA-Ile levels remained basal throughout the entire time course. OPDA levels, however, had already increased substantially and significantly by 1 h after PAMP treatment and remained elevated over time (Figure 6A). *OPR3*, *AOC1*, and *ACX1* transcript abundance also increased significantly 1 h after exposure to the PAMP (7.1-, 11-, and 3-fold) and remained elevated 3 h post-exposure, while declining 16 h post-exposure (Figure 6B). The abundance of all JA biosynthesis proteins also increased 1 h after flg22 treatment but more gradually and to a lesser degree, generally peaking 16 h after treatment (Figure 6B).

JOX2 transcripts were already elevated substantially and significantly at 1 h after PAMP treatment and remained high throughout the time course (Figure 6D). *IAR3* and *CYP94C1* transcript abundance increased in a similar manner after 1 h but decreased 3 h post-treatment and declined to basal levels 16 h after treatment (Figure 6D). The abundance of *CYP94B1* and *B3* transcripts did not increase above basal levels at any time point. The JOX2 and IAR3 protein levels increased significantly by 3 h, and were further elevated 16 h post-flg22 exposure in the former and were elevated 3 h and significantly 16 h in the latter case (Figure 6E). Levels of 12-Hydroxy-JA (12-OH-JA), the product of JA-Ile deconjugation and JA hydroxylation, already increased 1 h and further substantially and significantly 3 and 16 h after flg22 treatment (Figure 6A).

Measurements in the *myc234* mutant background corroborated these results. JA and JA-Ile levels increased substantially and significantly, peaking at 1 h (Ja-Ile) and 3 h (JA) post-treatment (maximum JA-Ile 12.1-fold at 1 h and JA 13.5-fold at 3 h after

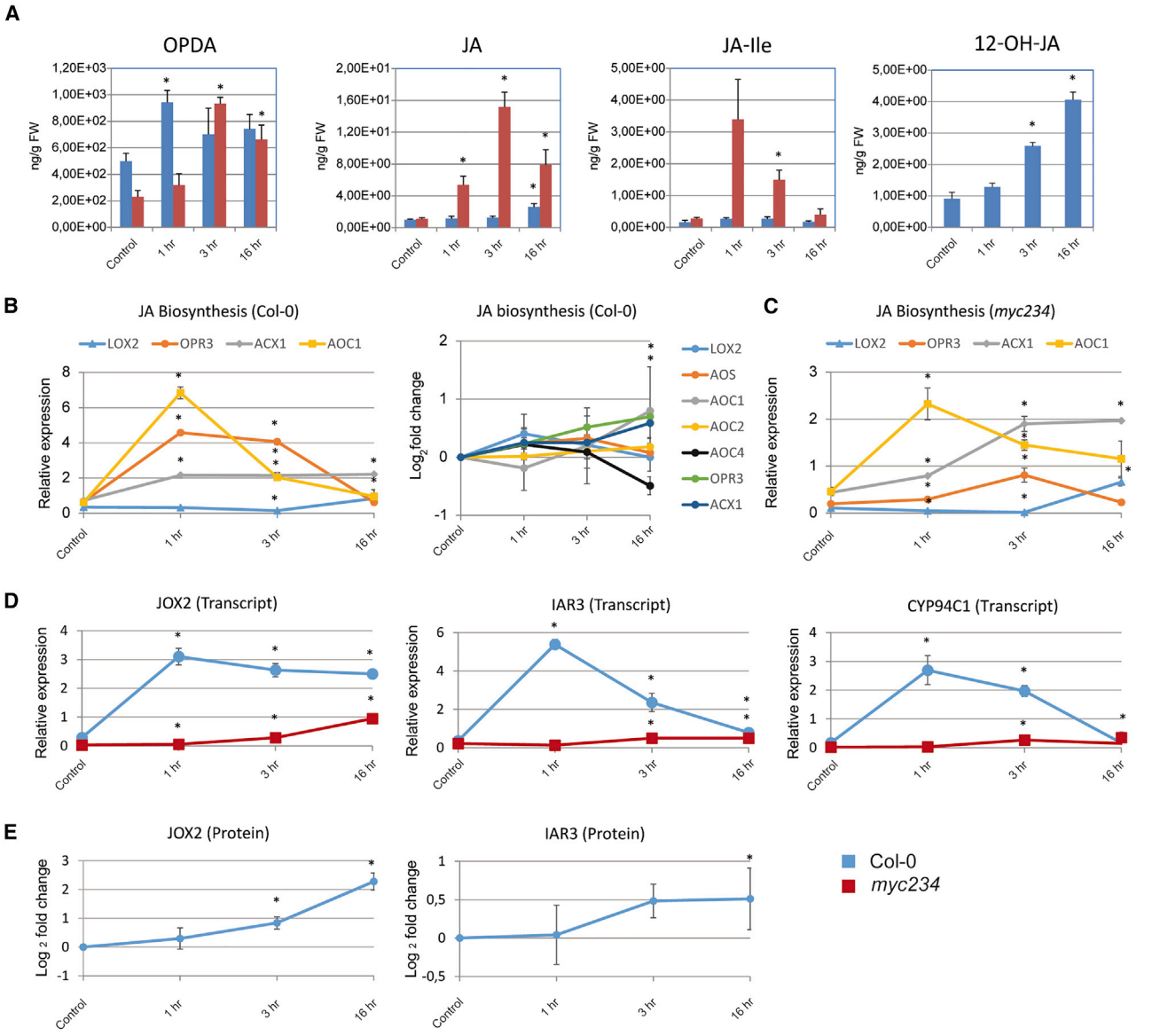

Figure 6. Hormone, Transcript, and Protein Abundance Profiles in the WT and *myc234* Plants at 1, 3, and 16 h after flg22 Treatment.

(A) Absolute quantification of phytohormones in Col-0 WT and myc234 mutant backgrounds using LC-MS. Bars represent mean of three biological replicates; standard error is given.

(B) qPCR-based transcript abundance profiling of selected JA biosynthesis genes in the WT. Bars represent means of six measurements (three biological replicates each measured twice), standard error is given. Right panel: targeted PRM-based quantification of all JA biosynthesis proteins in the WT. Quantification as described in Figure 5 for eight measurements (four biological replicates each measured twice).

(C) qPCR-based transcript abundance profiling of the same genes as in **(B)** in the myc234 mutant background.

(D) qPCR-based transcript abundance profiling of *JOX2*, *IAR3*, and *CYP94C1* in the WT and myc234 mutant backgrounds.

(E) Targeted PRM-based quantification of JOX2 and IAR3 proteins in the WT. Quantification as in Figure 5 for eight measurements (four biological replicates each measured twice). Stars represent statistically significant changes with a significance threshold of α = 0.05with respect to the untreated control. Two-sided *t*-test was used. See Supplemental Table 23 for all values.

flg22 stimulus) (Figure 6A). OPDA levels likewise increased after exposure to the PAMP, with a maximum increase of 4-fold at 3 h after flg22 perception (Figure 6A). JA biosynthesis gene expression showed a similar profile, yet transcript abundance was diminished in comparison with the wild type, presumably because MYC2 is a transcriptional activator of these genes (Zhang et al., 2020) (Figure 6C). This is direct evidence that JA synthesis and JA conjugation by JAR1, whose transcript showed statistically significant, slightly elevated abundance in both the wild type and the mutant throughout the time course, peaking at 16 h after flg22 perception, took place in response to flg22 independently of MYC2. JAR1 protein levels were also elevated and likewise peaked 16 h after PAMP exposure (0.3 $\log_2$ fold change).

We were then prompted to investigate the *IAR3* and *JOX2* promoter regions for MYC2 binding sites, and indeed two and three were identified as the top ranking hits, respectively. The transcript

levels of *IAR3* and *JOX2*, as well as *CYP94C1*, remained at nearly basal levels far below the wild type levels (albeit with a very slight statistically significant increase) in the *myc234* background (Figure 6D), confirming the transcriptional activation of these genes by MYC2.

SA accumulated after 1 h and levels remained elevated until 16 h after exposure in the wild type (Supplemental Table 23). The hormone hyperaccumulated in the triple knockout under standard growth conditions, as described previously (Nickstadt et al., 2004). Its abundance decreased markedly by 0.54- and 0.78-fold at 1 and 3 h, respectively, but increased at 16 h after flg22 perception, suggesting that JA signaling plays a role in SA accumulation in PTI and that it is an early one. The other phytohormones showed similar levels over time in both the wild type and the mutant (Supplemental Table 23). The amount of free IAA did not change dramatically, increasing slightly at earlier time points and decreasing as stated above at the 16-h time point, presumably because steady-state PTI was achieved. ACC/ET abundance increased by 1 h after exposure of the seedlings to the PAMP and remained elevated. ABA decreased 3 h after flg22 treatment and remained low throughout the time course, presumably because of its known antagonism with SA (Cao et al., 2011).

The abundances of *COI1*, *TPR1*, and *TPR3* transcripts showed a slight statistically significant increase over time, peaking at 16 h post-flg22 stimulus in both the wild type and mutant (Supplemental Table 23). This was also observed for the TPR3 protein in the wild type (0.46 $\log_2$ fold change). The auxin/IAA efflux carriers PIN3 and PIN7 both already showed a pronounced and significant decrease in transcript levels 1 h after flg22 treatment in wild type and the *myc234* background, and transcript levels remained well below the levels in untreated plants throughout the time course (Supplemental Table 23). The effect was somewhat diminished in the mutant. Downregulation was corroborated by the measurements of protein abundance; however, the decrease in transcript levels was significant and apparent after 3 h and protein levels reached a minimum 16 h post-flg22 treatment (Supplemental Table 23). This suggests a discrepancy in transcript and protein turnover rates that warrants further investigation and underscores a possibly important role of changes in auxin/IAA gradients in PTI already suggested by the deep proteomics results.

We also profiled changes in the abundance of some transcripts and all proteins in defense-related secondary metabolite synthesis pathways particularly those involved in IG biosynthesis, which are shown in Figure 5 boxed in orange, as well as the IGs I3M, 1MOI3M, and 4MOI3M (Supplemental Table 23). Transcript abundance increased significantly and substantially at 1 h and decreased slightly yet remained elevated 3 h after flg22 treatment. Interestingly, however, the transcript levels were not much elevated 16 h after PAMP exposure, showing a trend to return to untreated plant levels. This was the case in both the wild type and the triple *myc* knockout. An increase in protein levels was already visible at 1 h; levels increased pronouncedly and significantly at 3 h, and were elevated further 16 h after treatment with the PAMP, with the exception of CYP83A1, whose levels were diminished, as also reported above. These results again show differences in the temporal patterns of transcript and protein turnover and show that much of the secondary metabolite/defense compounds are presumably synthesized earlier than 16 h into PTI.

Measurement of the IGs themselves showed that I3M already decreased significantly and substantially in the wild type 1 h after exposure to flg22 and remained at comparably low levels throughout the time course. There was no significant change in 1MOI3M levels at any point post-PAMP treatment in either genotype. 4MOI3M amounts, however, decreased 1 and 3 h after treatment yet increased strongly 16 h after treatment in both the wild type and *myc234* mutant, and significantly so in the mutant. Interestingly the triple knockout mutant showed an almost complete absence of IGs, absolute levels being in the low pg/g FW.

In addition, we measured changes in the levels of the 20 proteinogenic amino acids and some others and found that levels of alanine, glycine, tryptophan, and taurine increased during the course of flg22 exposure (Supplemental Figure 19). The abundances of leucine, isoleucine, lysine, proline, and ornithine decreased over time after exposure.

DISCUSSION

Deep Proteomics Study of *Arabidopsis thaliana* Proteome

In this study, we elucidated the proteome landscapes of *Arabidopsis* plant and tissues throughout the lifecycle as well as during the immune response to a PAMP, quantifying close to 16 000 *Arabidopsis proteins*. Importantly, we placed an emphasis on remodeling of proteome architecture between these diverse biological scenarios to extrapolate genome-wide protein co-regulation and function. This approach has just recently been documented in humans (Kustatscher et al., 2019) and draws its power from deep coverage of the proteome as we have done here. In-depth sampling allowed quantitative measurement of all of the components of entire biochemical pathways, such as JA synthesis in PTI, protein complex components, such as RBF complexes, and protein co-expression of genes in local neighborhoods, such as CRKs, facilitating confident inference of protein abundance co-regulation and functional and temporal connections, for instance, in seed development and dormancy, the establishment, maintenance, and deconstruction of the photosynthetic machinery, and in senescence and abscission.

Our study provides one of three recently published *A. thaliana* tissue atlantes (Mergner et al., 2020; Zhang et al., 2019; our study). Interestingly, all three studies quantified approximately the same number of proteins (18 210, 15 514, and 15 926). Despite their different methods, each with great sampling depth, Mergner et al., 2020 and Zhang et al., 2019 did not delve much deeper into the entire *Arabidopsis* proteome than Baerenfaller et al. (2008) did more than 10 years ago (or as a matter of fact the authors of other deep proteomics studies in plants). In their classic study individual sampling depth was modest; however, they utilized more than 1300 low-resolution LC-MS measurements to quantify nearly 15000 proteins. All studies showed a

similar impact of transcript abundance on the detection of cognate proteins (Figure 3, Mergner et al., 2020; Figure 2C, Baerenfaller et al., 2008; Figure 1C, this study); however, we show that protein size has a more pronounced effect, presumably because small proteins will generate fewer tryptic peptides amenable to MS detection. It may also be a possibility that very small proteins migrate to a position in or below the Coomassie front on the SDS gel and may thus be lost in our GeLC-MS method. Also, transcription factors and nuclear proteins, whose expression may be highly transient and biological context specific, were conspicuously overrepresented in the missing proteome (Supplemental Figure 4). Capturing these proteins could require even more exhaustive sampling of different organs at all developmental stages than done by Mergner et al. (imagine for example the diversity of the 12 stages of organ development in the floral bud [Bowman et al., 1989; Smyth et al., 1990]) and under different environmental conditions, and even then may escape detection. Indeed, the more than 8000 proteins we identified in the context of flg22 treatment did not substantially increase the amount of total proteins previously identified in the plant tissues (Supplemental Figure 7). Also, the proteomics ruler method allowed us to quantify proteins with fewer than 100 copies per cell, which is in general agreement with limits of quantitation of modern large-scale proteomics studies in humans (Bekker-Jensen et al., 2017) and similar to those we calculated from the data of Mergner et al. Together, this suggests that even more comprehensive sampling of the *A. thaliana* proteome may be difficult with current technologies.

Nevertheless, these three studies together have almost completely mapped the *A. thaliana* proteome. A very recent study described comparative deep proteomics in 100 taxonomically distinct organisms in all kingdoms of life (Müller et al., 2020). These exciting studies in the last year have paved the way for mature proteomics in *Arabidopsis* and other plants and ushered in a modern era of true comparative functional genomics.

In addition to the prevalent known artificial and biologically occurring modifications, amino acid substitutions were found to be common. Such exchanges, which are generally caused by ribosome infidelity and have a number of biological implications, have been reported previously in human cell lines (Chick et al., 2015), human tissues (Bagwan et al., 2018), and in *Escherichia coli* and yeast in detail (Mordret et al., 2019). The latter study defines exchanges as near cognate errors when two of the three bases between the error-bearing origin and destination codon match and as non-cognate errors when there is no such match between possible error-bearing origin and destination codons. Interestingly, five of the eight substitutions we found to be abundant in *Arabidopsis* (Asn → Met, Ala → Asp, Pro → Glu, Asp → Asn, and Glu → Gln) were also abundant in yeast but not *E.coli*, and three (Ala → Asp, Asp → Asn, and Glu → Gln) were near cognate errors, suggesting conserved patterns of translational error in eukaryotes, a possible method of generating random phenotype variants in genetically identical organisms (Mordret et al., 2019). This phenomenon may also highlight the limitations of searching protein databases derived from reference genomes with proteomics data.

Root Proteome

The root is a highly specialized, plastic tissue that confers structural stability to the above ground portion of the plant and is responsible for the uptake of nutrients and water from the soil. Thus, it exudes a number of metabolites, peptides, and proteins that allow it to interact with the rhizobiome. The function of the root-specific proteins in cluster 3 are well documented. Interestingly the transcription factors and proteins that pertain to hormone signaling in the developing root (Paez Valencia et al., 2016) were not overly prominent among the set of cluster proteins.

Many of the membrane trafficking cluster 13 proteins were abundant in fast growing tissues, mainly the roots but also in the stem and flowers. Vesicle trafficking is preeminent in the targeted deposition of new cell wall material in the clear zone at the apex of tip growing cells as is the formation of an apical actin structure. Our results suggest that at leastsome of the molecular players in the growing root tip may play other very different roles in various organs.

Seed Proteome

The proteins in cluster 7 include many of the proteins involved in ABA-dependent regulation of seed development. The amount of ABI5, a positive regulator of ABA signaling is post-translationally controlled by AFP1, presumably by promoting its degradation by the proteasome (Lynch et al., 2017). The high ABI5 to AFP1 ratio measured in post-mature seeds indicates high ABA levels and ABI5 activity in the induction and maintenance of dormancy. ABI5 is a positive regulator of ABA signaling , which not only functions in the induction and maintenance of seed dormancy (Finkelstein et al., 2008) but also represses the flowering transition (Wang et al., 2013). A handful of proteins have been reported to target ABI5 for degradation and thus negatively impact the ABA response, including AFP1 (Lopez-Molina et al., 2003) and DWA2 (Lee et al., 2010). Both proteins had distinct abundance patterns:. AFP1 was most abundant in ripe brown siliques and DWA2 abundance was elevated in young roots, young stems, and early flowers/floral buds wherein it presumably mediates ABI5 degradation to induce flowering. These results suggest that different developmental and tissue-specific mechanisms post-translationally control ABI5 levels and ABA activity.

ABA and DOG1 pathways converge on PP2C phosphatases such as AHG1 to suppress germination (Nee et al., 2017). DOG1 and the PP2Cs RDO5 and AHG1 wereamong the most abundant measured proteins, suggesting a possibly dominant role of this pathway over ABA signaling in seed dormancy. In addition, two other PP2Cs (AT3G15260 and AT4G31860 of the F and I clades, respectively) previously not known to be involved in seed development also accumulated to very high levels, implicating that they are involved in the same processes. The abundance of RD26/ANAC72 (AT4G27410) and its two closest homologs ANAC19 (AT1G52890) and ANAC03 (AT3G15500), as well as two other NAC transcription factors, ANAC02 (AT3G15510) and ANAC14 (AT1G33060), increased specifically and significantly in seeds, particularly in post-mature seeds (brown siliques). *RD26* and homologs have been shown to be ABA responsive (Fujita et al., 2004) and to be expressed ubiquitously in *Arabidopsis* vegetative tissues in response to

drought and salt stress (Tran et al., 2004; Nakashima et al., 2012) and coronatine (Zheng et al., 2012). They are also known to play a role in JA (Bu et al., 2008) and brassinosteroid signaling (Ye et al., 2017) as well as leaf senescence (Takasaki et al., 2015). The seed-specific accumulation of these NACs in the absence of stress indicates that they may play a previously unknown role in the onset and maintenance of seed desiccation tolerance. No seed-specific or reproductive phenotype has been reported for the respective single mutants of these NAC genes, suggesting a possible functional redundancy.

Ribosomal Proteins in Development

The deep proteome coverage of our approach allowed us to identify entire RBF protein complexes, all of whose members had the same expression pattern. The RBF complexes were part of the SSU processome or the pre-60S pre-ribosomal particle, and mutation of many RBF constituents has been found to lead to aberrant gametophyte development. This suggests that, in particular, these complexes regulate gametophyte development in early flowers in the context of ribosome biogenesis and translation, underscored by the their much more conserved, significant expression pattern as opposed to RPs in general. It has been reported that the transcripts of several of these genes are especially abundant in developing tissues, such as young roots, stems, and flowers (Missbach et al., 2013). Furthermore, the extensive physical interaction between RPs and RBFs and the protein abundance pattern found here may indicate that these particular isoforms assemble ribosomes specific to young roots, young stems, and early flowers/floral buds with possible functions specific to these tissue states.

Senescence and Abscission

It is no surprise that a large number of antioxidant proteins and proteins involved in redox regulation and ROS scavenging increased in abundance as aging progressed, peaking in leaves, cauline leaves, and flowers/siliques during senescence. Chlorophyll and carotenoid catabolism are central aspects of leaf senescence, and CYP89A9 is important in this respect by catalyzing the oxidative deformylation of FCCs to dioxibilin-type FDCCs and ultimately leading to the accumulation of NDCCs (Christ et al., 2013). *CYP89A2* has been shown to be co-expressed with *CYP89A9* (Obayashi et al., 2009), and we have observed this here for the cognate proteins. In addition to these two CYPs, 10 other CYP71 clan members had the same protein abundance pattern as cluster 10 proteins. This makes it likely that a larger number of CYPs play undescribed roles in chlorophyll catabolism, as was also speculated by Christ et al.

We detected six CRKs showing the characteristic abundance pattern associated with senescence. This RLK gene family consists of 44 members, all located in close proximity on chromosome 4 with a host of different physiological functions (Wrzaczek et al., 2010; Burdiak et al., 2015). Their extracellular regions have two conserved DUF domains, each with four cysteine residues that are potential targets for thiol redox regulation. Members of the gene family have been shown to be expressed at the transcript and protein levels in response to pathogen challenge, flg22, and SA, underpinning a potential role in immunity (Wrzaczek et al., 2010; Yadeta et al., 2017). Transcripts of five of the six CRKs we identified were also significantly upregulated after ozone treatment (Wrzaczek et al., 2010). Collectively, these processes and senescence all involve ROS, although the spatio-temporal mechanisms of ROS production, interaction, and signaling in the senescence syndrome are not well understood. A probable ROS-dependent role of CRK5 in cell death and senescence has been documented (Burdiak et al., 2015). HYDRGEN-PEROXIDE-INDUCED CA^{2+} INCREASES 1 (HPCA1), an LRR-RLK with extracellular cysteine residues, has been recently shown to sense H_2O_2 and induce stomatal closure (Wu et al., 2020).

Arabidopsis floral organ abscission, which is the culmination of petal senescence and nutrient remobilization for fruit ripening and ultimately release, is a well-studied model of general abscission processes (Patharkar and Walker, 2018). We found that most of the components of the abscission signaling cascade increased in abundance in flowers as they aged and set seeds in siliques after fertilization. It has been shown that the same mechanisms also act in *Arabidopsis* cauline leaf abscission in response to drought (Patharkar and Walker, 2016), and indeed plants commonly shed their leaves in response to various environmental stimuli. However, leaf abscission is not known to be on a developmental clock and *Arabidopsis* does not abscise rosette leaves (Stenvik et al., 2006), making our findings intriguing and worth of further investigations.

ABA plays a major role in fruit ripening (Jia et al., 2011) and the leaf senescence syndrome (Song et al., 2016), yet its role in abscission is debated. ABA promotes ET biosynthesis during the later stages of fruit ripening in tomato (Zhang et al., 2009) and ET is known to be a regulator of abscission in *Arabidopsis* (Patterson and Bleecker, 2004). ABA is also a key hormone in plant response to drought (Huang et al., 2008). *HAE*, *HLS2*, and *IDA* expression in *Arabidopsis* seedlings is induced by ABA and to a lesser extent by ET (eFP browser [Goda et al., 2008]). It is possible that the elevated ABA and ET levels over the course of senescence led to the accumulation of the abscission signaling proteins in rosette and cauline leaves. Therefore, one may speculate on other possible yet unknown functions of this signaling module outside of organ abscission.

Photosynthesis and Primary Metabolism in PTI

The tissue and developmental abundance profile of cluster 11 proteins implicates them in chloroplast biogenesis prevalent in young plants. The proteins of the photosynthetic apparatus are abundant in green tissues in nearly all developmental stages, beginning in the cotyledons of the young seedling before photoautotrophy. This can be seen in the abundance profile of the proteins in cluster 8, which decreases in leaves in the later senescent stages concomitantly with an increase in abundance of proteins in cluster 10 that facilitate disassembly of the apparatus and pigment degradation.

It is known that pathogen infection leads to inhibition of photosynthesis and that this is an active response of the plant to the invading pathogen. Downregulation of a host of genes related to the light-dependent reactions, particularly PSII, and photosynthetic activity parameters have recently been reported to be dependent on constitutive MPK3/MPK6 activation in

effector-triggered immunity (Su et al., 2018). The resulting increase in chloroplast-localized ROS is hypothesized to support programmed cell death in the hypersensitive response. Measurement ofphotosynthetic parameters upon exposure to 100 nM flg22 for up to 24 h or infiltration with a *Pst* DC3000 strain that lacks a type III secretion system to deliver effectors in this study indicated that downregulation of photosynthesis does not occur during PTI, which features only transient MPK3/MPK6 activation. A previous proteomics study, however, found downregulation of some photosynthetic proteins and non-photochemical quenching 2 h after flg22 treatment (100 nM–10 μM) and decreased electron flux through PSII upon 7 days of exposure, suggesting that inhibition of photosynthesis may occur in some PTI scenarios (Gohre et al., 2012). This is in line with our findings where plants were exposed to 1 μM flg22 for 16 h. Conceivably, higher flg22 doses may lead to prolonged MPK3/MPK6 activation and photosynthetic inhibition in PTI, consistent with our finding that the abundance of both MPK3 and MPK6 increased somewhat in the discovery proteomics resultsupon PAMP exposure (Supplemental Table 14).

Jasmonate Metabolism in PTI

The induction of PTI downstream of FLS2 binding of flg22 is a commonly accepted model of bacteria-induced basal immunity in plants. In addition to FLS2, bacteria are also recognized by other pattern recognition receptors, such as EF-TU RECEPTOR and others to induce multiple partially overlapping responses.

The importance of SA and JA in resistance to biotrophs and necrotrophs, respectively, as well as their generally antagonistic modes of action are well documented (Pieterse et al., 2012). Both hormones interact and play roles in flg22-induced PTI (Denoux et al., 2008; Yi et al., 2014; Hillmer et al., 2017; Mine et al., 2017). SA accumulation is essential for flg22-triggered defenses (Tsuda et al., 2008). The suppressive effect of SA on JA levels has been extensively explored and shown to be NPR1 dependent in *Pst* DC3000-infected *Arabidopsis* plants (Spoel et al., 2003) and integral to the trade-off between defense against biotrophic and necrotrophic pathogens (Spoel et al., 2007). However, most of this interplay occurs downstream of JA synthesis at the level of inhibition of JA-responsive gene transcription by transcriptional regulators, primarily WRKY70, TGAs and ORA59 (Li et al., 2004; Leon-Reyes et al., 2010; Shim et al., 2013; Van der Does et al., 2013; Zander et al., 2014).

Control of JA response by JA conjugation and catabolism is known in the context of the wound response and fungal infection. JA is conjugated to isoleucine by JAR1, producing the bioactive JA compound JA-Ile. Two major pathways of JA-Ile removal have been characterized. Two-step ω-oxidation of JA-Ile to 12-OH-JA-Ile and 12-COOH-JA-Ile by the cytochrome P450 oxidases CYP94B1/B3 and CYP94C1, respectively, was described in the wound response (Heitz et al., 2012; Koo et al., 2014) where it has been shown to be the more prominent pathway (Smirnova et al., 2017). Deconjugation of 12-OH-JA-Ile to 12-OH-JA by the amidohydrolase IAR3/ILL6 is another route in this pathway adding additional metabolic complexity (Widemann et al., 2013; Zhang et al., 2016). Direct inactivation of JA-Ile via deconjugation by IAR3 and subsequent oxidation to 12-OH-JA by JA oxidases, primarily JOX2, is the second pathway discovered more recently, which plays a more important role in the response to necrotrophic pathogen infection (Caarls et al., 2017; Smirnova et al., 2017). We found that this second pathway is also activated by flg22. Furthermore, expression of IAR3 and JOX2 and the pathway itself are primarily under the control of MYC2 in PTI. The major lines of evidence for this model t are as follows: (1) Absolute levels of the JA intermediate OPDA were very high (μg/g FW) and increased by more than four-fold after flg22 treatment in both the wild type and the *myc234* background. (2) The abundance of selected transcripts and all proteins in the JA synthesis pathway increased after induction of PTI in both genotypes. JA and JA-Ile levels were very low and did not increase significantly after flg22 treatment in the wild type; however, they were strongly elevated in the *myc234* mutant suggesting that the JA synthesis pathway is induced but that JA and JA-Ile clearance is prevalent dependent on MYC2. (3) IAR3 and JOX2 were among the transcripts and proteins with the most significantly increased fold change in abundance after flg22 treatment in the wild type. In the triple mutant background, however, transcript abundance was barely elevated above basal levels. *CYP94B1/B3* transcript levels did not increase above basal levels. (4) 12-OH-JA accumulated in the wild type afterflg22 treatment. This indicates that catabolism of the phytohormone and its bioactive conjugate by IAR3 and JOX2 is active in PTI and dependent on MYC2. These results lead us to hypothesize that depletion of JA-Ile and JA via deconjugation and subsequent modification by IAR3 and JOX2, respectively, also play an important role in control of the JA pathway in defense against biotrophs, in addition to their role against the necrotrophic fungus *Botrytis cinerea* (Figure 7) (Caarls et al., 2017). In contrast, the two-step ω-oxidation pathway does not seem to be important in this context because *CYP94B1* and *B3* transcripts did not increase above basal levels. JA/JA-Ile clearance is presumably in some type of equilibrium with JA synthesis, and it has been reported that the JA pathway is integral to PTI induction and SA accumulation via EDS5 (Mine et al., 2017). The involvement of JA signaling in SA accumulation is underscored in our data by the diminished SA levels in the *myc234* background at the earlier time points (1 and 3 h after flg22 exposure). Thus, consistent with a previous report (Spoel et al., 2003), our data could reconcile significant induction of the JA synthesis pathway components and known SA-JA antagonism at the level of transcriptional regulation.

Auxin/IAA Homeostasis in PTI

Auxins have established functions in plant immunity. Free IAA and IAA signaling both increase plant susceptibility to biotrophic pathogens (Kunkel and Harper, 2018), whereas IAA acts synergistically with JA in resistance to necrotrophic pathogens (Qi et al., 2012). Flg22 induces transcription of a microRNA, miR393, that targets the auxin receptor TRANSPORT INHIBITOR RESPONSE 1 (TIR1), thereby dampening auxin signaling (Navarro et al., 2006). Free IAA levels were not reported to change dramatically in response to flg22 (Navarro et al., 2006) nor to *Pst* DC3000 infection or SA (Qi et al., 2012). We also observed a slight but significant decrease after 16 h of

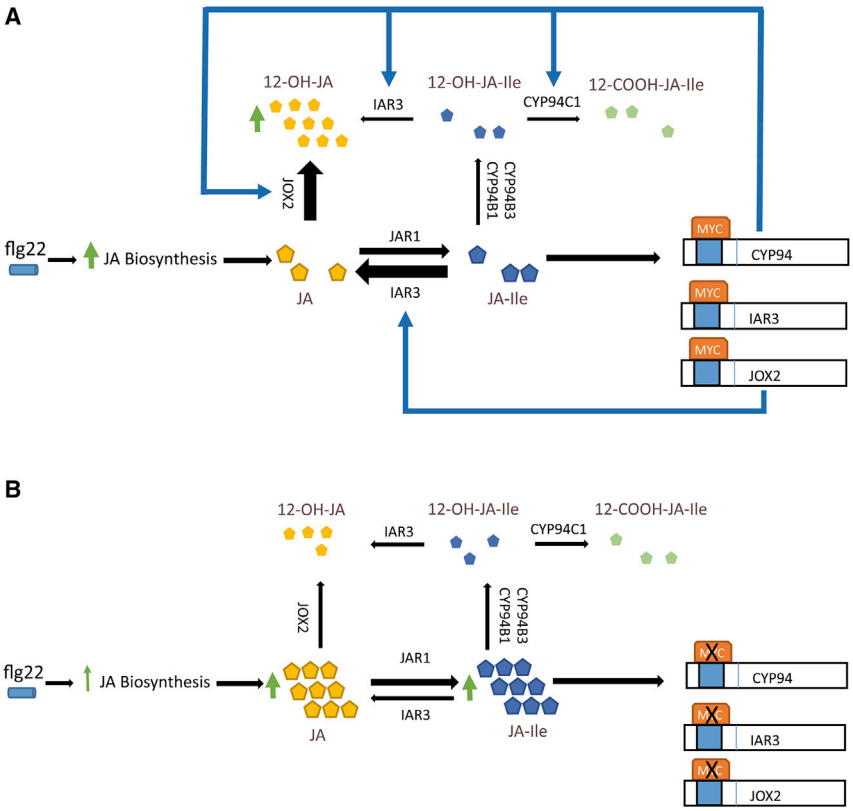

Figure 7. A MYC2-Dependent Negative Feedback Loop Controls JA-Ile and JA Levels in Equilibrium with JA Synthesis in Response to Biotrophic Pathogens.

(A) Flg22 induces JA synthesis and conjugation to isoleucine. The bioactive compound JA-Ile stimulates JA signaling and gene expression including expression of MYC2. MYC2 is a transcriptional activator of many JA-responsive genes and induces transcription of *IAR3*, *JOX*, and *CYP94C1*. Although it has been reported that transcriptional activation of *CYP94B1* and *B3* is also controlled by MYC2 during wounding (Zhang et al., 2020), we did not detect elevated transcript levels after flg22 treatment. This indicates that the indirect pathway to 12-OH-JA via ω-oxidation of JA-Ile does not play a major role in PTI. IAR3 and JOX2 proteins accumulate and deconjugate and hydroxylate JA-Ile and JA, respectively, clearing these compounds and leading to the accumulation of 12-OH-JA.

(B) In the absence of MYC2 (*myc234* knockout), *JOX2* and *IAR3* are not expressed, and JA-Ile and JA are not catabolized and do not accumulate.

flg22 treatment, presumably by downregulation of the IAM pathway by a decrease in the abundance of AMIDASE1 (AMI1) when steady-state PTI was reached. IAA is synthesized primarily from tryptophan through several biosynthetic pathways, and tryptophan also channels into defense compound synthesis, especially indolic glucosinolates and camalexin. I3M is converted to 4MOI3M by CYP81F2 and then hydrolyzed by PEN2. Our time-course profiling of IG levels corroborate results reported by Clay et al. (2009). The strong increase of 4MOI3M levels at 16 h after flg22 stimulus warrants further investigation, although both CYP81F2 and PEN2 protein levels were decreased at this time point. Thus, branching points in tryptophan/IAA biosynthesis pathways, particularly indole-3-acetaldoxime (IAOx) (Sugawara et al., 2009) may represent an important nexus in the growth defense trade-off.

It is known that JA induces tryptophan, IG, and auxin biosynthesis upon *Alternaria brassicicola* (a necrotrophic pathogen) infection, leading to increased free IAA (Qi et al., 2012). In our study, however, JA and JA-Ile levels remained basal. Notably, we measured a significant increase in the abundance of ET biosynthesis proteins ACC OXIDASE 2 (ACO2) and 1-AMINOCYCLOPROPANE-1-CARBOXYLATE SYNTHASE 7 (ACS7) and a significant (more than five-fold) increase of ET, 16 h after flg22 treatment. Clay et al. (2009) reported that ET also mediates expression of tryptophan and IG biosynthesis pathway transcripts via MYB transcription factors in the flg22 response. Our results are consistent with the data from Clay et al. (2009) and suggest that the tryptophan, IG, and auxin biosynthesis pathways are controlled by both ET and JA in different immune responses. These two hormones are generally synergistic, posing new questions about the role of JA in the flg22 response.

Auxins are transported directionally from cell to cell by a polar transport system with many components (Friml, 2003). Indeed, the distribution and local IAA concentration have a more profound impact on cellular processes than absolute IAA levels or aspects of synthesis and catabolism (Teale et al., 2006), and auxin transport mutants have been reported to be defective in mounting SAR (Truman et al., 2010a). Consistent with this, we found that the abundance of two auxin efflux carriers, PIN3 and PIN7, decreased and that of auxin influx carrier AUX1 increased after flg22 treatment. This suggests that IAA transport and local IAA gradients also play an important role in the defense against both biotrophic and necrotrophic pathogens (Qi et al., 2012).

METHODS

For a detailed description of methods and optimization see the Supplemental Methods and Data. In brief, proteins were extracted from *Arabidopsis thaliana* suspension cultures or soil-grown plants and tissues with 4% SDS, separated into five bands by SDS–PAGE, in-gel digested and measured on an Orbitrap Velos Pro mass spectrometer with a conventional DDA scan strategy using a 50 cm C18 liquid chromatography column and an extended gradient of 9 h. MS data were searched using the Mascot and Andromeda search engines. Search results were concatenated and peptides and proteins identified with global FDR thresholds of 0.01 in the Scaffold software. Proteins were quantified by way of PSM counting. For PRM, proteins were extracted with 4% SDS, digested with an optimized FASP protocol, and peptides measured on a QExactive Plus mass spectrometer. Up to three proteotypic peptide m/z per protein were targeted, and peptides and proteins

were identified using the Mascot search engine. Data analysis and AUC quantification of six fragment ions was done using the Skyline software (Pino et al., 2020). Statistical significance of protein fold changes was inferred at a threshold of 0.05 if one of the quantified peptides showed a significant test result.

qPCR was performed using the EvaGreen Kit from Bio&Sell according to the manufacturer's instructions, and phytohormone and amino acid measurements were performed according to (Ziegler et al., 2014).

Bioinformatics analysis including GO analysis and pathway visualization and mapping was done using DAVID (Huang da et al., 2009), MapMan (Thimm et al., 2004), and STRING (Szklarczyk et al., 2019); PTM analysis was done with MSFragger (Kong et al., 2017). Multivariate data analysis was done with the m-fuzz R package (Kumar and Futschik, 2007) in the case of fuzzy c-means clustering, and hierarchical clustering and PCA were performed with Perseus (Tyanova et al., 2016).

Both the raw and meta data produced in this study are available to the general public (via ProteomeXchange with identifier PXD019330 and PXD021724).

SUPPLEMENTAL INFORMATION

Supplemental Information can be found online at *Molecular Plant Online*.

FUNDING

We thank the Leibniz Association for support and funding. Mohammad Abukhalaf is funded by DFG grant HO 5063/2-1. Mohamed Ayash is funded by DFG 400681449/GRK2498. This work was also supported by de.NBI (FKZ 031 A 534A), a project of the BMBF (Bundesministerium für Bildung und Forschung).

AUTHOR CONTRIBUTIONS

Conceptualization, W.H.; Methodology, W.H., P.M., D.T., S.N., and J.Z.; Validation, N.T. and J.L.; Formal Analysis, W.H., M.B., M. Abukhalaf, P.M., D.T., M. Ayash, M.R.A.S., A.H., J.Z., and T.H.; Investigation, M.B., M. Abukhalaf, P.M., D.T., M. Ayash, N.T., M.R.A.S., C.P., A.H. and J.Z.; Data Curation, S.N.; Writing – Original Draft, W.H.; Writing – Review & Editing, W.H.; Visualization, M. Abukhalaf and W.H.; Supervision, W.H., S.N., and J.L.; Project Administration, W.H.; Funding Acquisition, W.H.

ACKNOWLEDGMENTS

The manuscript is dedicated to Prof. em. Dr. Dierk Scheel who was always a tremendous source of inspiration. No conflict of interest declared.

Received: May 18, 2020
Revised: August 21, 2020
Accepted: September 25, 2020
Published: September 28, 2020

REFERENCES

Agarwal, P., Kapoor, S., and Tyagi, A.K. (2011). Transcription factors regulating the progression of monocot and dicot seed development. Bioessays **33**:189–202.

Ahn, C.S., Cho, H.K., Lee, D.H., Sim, H.J., Kim, S.G., and Pai, H.S. (2016). Functional characterization of the ribosome biogenesis factors PES, BOP1, and WDR12 (PeBoW), and mechanisms of defective cell growth and proliferation caused by PeBoW deficiency in *Arabidopsis*. J. Exp. Bot. **67**:5217–5232.

Baerenfaller, K., Grossmann, J., Grobei, M.A., Hull, R., Hirsch-Hoffmann, M., Yalovsky, S., Zimmermann, P., Grossniklaus, U., Gruissem, W., and Baginsky, S. (2008). Genome-scale proteomics reveals *Arabidopsis thaliana* gene models and proteome dynamics. Science **320**:938–941.

Bagwan, N., Bonzon-Kulichenko, E., Calvo, E., Lechuga-Vieco, A.V., Michalakopoulos, S., Trevisan-Herraz, M., Ezkurdia, I., Rodriguez, J.M., Magni, R., Latorre-Pellicer, A., et al. (2018). Comprehensive quantification of the modified proteome reveals oxidative heart damage in mitochondrial heteroplasmy. Cell Rep. **23**:3685–3697 e3684.

Bekker-Jensen, D.B., Kelstrup, C.D., Batth, T.S., Larsen, S.C., Haldrup, C., Bramsen, J.B., Sorensen, K.D., Hoyer, S., Orntoft, T.F., Andersen, C.L., et al. (2017). An optimized shotgun strategy for the rapid generation of comprehensive human proteomes. Cell Syst. **4**:587–599.e4.

Bigeard, J., Colcombet, J., and Hirt, H. (2015). Signaling mechanisms in pattern-triggered immunity (PTI). Mol. Plant **8**:521–539.

Bleecker, A.B., and Patterson, S.E. (1997). Last exit: senescence, abscission, and meristem arrest in *Arabidopsis*. Plant Cell **9**:1169–1179.

Blilou, I., Xu, J., Wildwater, M., Willemsen, V., Paponov, I., Friml, J., Heidstra, R., Aida, M., Palme, K., and Scheres, B. (2005). The PIN auxin efflux facilitator network controls growth and patterning in *Arabidopsis* roots. Nature **433**:39–44.

Boudsocq, M., Willmann, M.R., McCormack, M., Lee, H., Shan, L., He, P., Bush, J., Cheng, S.H., and Sheen, J. (2010). Differential innate immune signalling via Ca(2+) sensor protein kinases. Nature **464**:418–422.

Bowman, J.L., Smyth, D.R., and Meyerowitz, E.M. (1989). Genes directing flower development in *Arabidopsis*. Plant Cell **1**:37–52.

Breeze, E., Harrison, E., McHattie, S., Hughes, L., Hickman, R., Hill, C., Kiddle, S., Kim, Y.S., Penfold, C.A., Jenkins, D., et al. (2011). High-resolution temporal profiling of transcripts during *Arabidopsis* leaf senescence reveals a distinct chronology of processes and regulation. Plant Cell **23**:873–894.

Bu, Q., Jiang, H., Li, C.B., Zhai, Q., Zhang, J., Wu, X., Sun, J., Xie, Q., and Li, C. (2008). Role of the *Arabidopsis thaliana* NAC transcription factors ANAC019 and ANAC055 in regulating jasmonic acid-signaled defense responses. Cell Res. **18**:756–767.

Burdiak, P., Rusaczonek, A., Witon, D., Glow, D., and Karpinski, S. (2015). Cysteine-rich receptor-like kinase CRK5 as a regulator of growth, development, and ultraviolet radiation responses in *Arabidopsis thaliana*. J. Exp. Bot. **66**:3325–3337.

Byrne, M.E. (2009). A role for the ribosome in development. Trends Plant Sci. **14**:512–519.

Caarls, L., Elberse, J., Awwanah, M., Ludwig, N.R., de Vries, M., Zeilmaker, T., Van Wees, S.C.M., Schuurink, R.C., and Van den Ackerveken, G. (2017). *Arabidopsis* JASMONATE-INDUCED OXYGENASES down-regulate plant immunity by hydroxylation and inactivation of the hormone jasmonic acid. Proc. Natl. Acad. Sci. U S A **114**:6388–6393.

Cao, F.Y., Yoshioka, K., and Desveaux, D. (2011). The roles of ABA in plant-pathogen interactions. J. Plant Res. **124**:489–499.

Chen, C.N., Chen, H.R., Yeh, S.Y., Vittore, G., and Ho, T.H. (2009). Autophagy is enhanced and floral development is impaired in AtHVA22d RNA interference *Arabidopsis*. Plant Physiol. **149**:1679–1689.

Chi, H., Liu, C., Yang, H., Zeng, W.F., Wu, L., Zhou, W.J., Wang, R.M., Niu, X.N., Ding, Y.H., Zhang, Y., et al. (2018). Comprehensive identification of peptides in tandem mass spectra using an efficient open search engine. Nat. Biotechnol. https://doi.org/10.1038/nbt.4236.

Chick, J.M., Kolippakkam, D., Nusinow, D.P., Zhai, B., Rad, R., Huttlin, E.L., and Gygi, S.P. (2015). A mass-tolerant database search identifies a large proportion of unassigned spectra in shotgun proteomics as modified peptides. Nat. Biotechnol. **33**:743–749.

Cho, H.K., Ahn, C.S., Lee, H.S., Kim, J.K., and Pai, H.S. (2013). Pescadillo plays an essential role in plant cell growth and survival by modulating ribosome biogenesis. Plant J. **76**:393–405.

Choi du, S., Lim, C.W., and Hwang, B.K. (2016). Proteomics and functional analyses of *Arabidopsis* nitrilases involved in the defense response to microbial pathogens. Planta **244**:449–465.

Christ, B., Sussenbacher, I., Moser, S., Bichsel, N., Egert, A., Muller, T., Krautler, B., and Hortensteiner, S. (2013). Cytochrome P450 CYP89A9 is involved in the formation of major chlorophyll catabolites during leaf senescence in *Arabidopsis*. Plant Cell **25**:1868–1880.

Clay, N.K., Adio, A.M., Denoux, C., Jander, G., and Ausubel, F.M. (2009). Glucosinolate metabolites required for an *Arabidopsis* innate immune response. Science **323**:95–101.

Davies, R.T., Goetz, D.H., Lasswell, J., Anderson, M.N., and Bartel, B. (1999). IAR3 encodes an auxin conjugate hydrolase from *Arabidopsis*. Plant Cell **11**:365–376.

Dekker, C., Roe, S.M., McCormack, E.A., Beuron, F., Pearl, L.H., and Willison, K.R. (2011). The crystal structure of yeast CCT reveals intrinsic asymmetry of eukaryotic cytosolic chaperonins. EMBO J. **30**:3078–3090.

Denoux, C., Galletti, R., Mammarella, N., Gopalan, S., Werck, D., De Lorenzo, G., Ferrari, S., Ausubel, F.M., and Dewdney, J. (2008). Activation of defense response pathways by OGs and Flg22 elicitors in *Arabidopsis* seedlings. Mol. Plant **1**:423–445.

Dharmasiri, S., Swarup, R., Mockaitis, K., Dharmasiri, N., Singh, S.K., Kowalchyk, M., Marchant, A., Mills, S., Sandberg, G., Bennett, M.J., et al. (2006). AXR4 is required for localization of the auxin influx facilitator AUX1. Science **312**:1218–1220.

Duncan, O., Trosch, J., Fenske, R., Taylor, N.L., and Millar, A.H. (2017). Resource: mapping the *Triticum aestivum* proteome. Plant J. **89**:601–616.

Finkelstein, R., Reeves, W., Ariizumi, T., and Steber, C. (2008). Molecular aspects of seed dormancy. Annu. Rev. Plant Biol. **59**:387–415.

Friml, J. (2003). Auxin transport—shaping the plant. Curr. Opin. Plant Biol. **6**:7–12.

Fujita, M., Fujita, Y., Maruyama, K., Seki, M., Hiratsu, K., Ohme-Takagi, M., Tran, L.S., Yamaguchi-Shinozaki, K., and Shinozaki, K. (2004). A dehydration-induced NAC protein, RD26, is involved in a novel ABA-dependent stress-signaling pathway. Plant J. **39**:863–876.

Futschik, M.E., and Carlisle, B. (2005). Noise-robust soft clustering of gene expression time-course data. J. Bioinform Comput. Biol. **3**:965–988.

Gavin, A.C., Aloy, P., Grandi, P., Krause, R., Boesche, M., Marzioch, M., Rau, C., Jensen, L.J., Bastuck, S., Dumpelfeld, B., et al. (2006). Proteome survey reveals modularity of the yeast cell machinery. Nature **440**:631–636.

Gavin, A.C., Bosche, M., Krause, R., Grandi, P., Marzioch, M., Bauer, A., Schultz, J., Rick, J.M., Michon, A.M., Cruciat, C.M., et al. (2002). Functional organization of the yeast proteome by systematic analysis of protein complexes. Nature **415**:141–147.

Goda, H., Sasaki, E., Akiyama, K., Maruyama-Nakashita, A., Nakabayashi, K., Li, W., Ogawa, M., Yamauchi, Y., Preston, J., Aoki, K., et al. (2008). The AtGenExpress hormone and chemical treatment data set: experimental design, data evaluation, model data analysis and data access. Plant J. **55**:526–542.

Gohre, V., Jones, A.M., Sklenar, J., Robatzek, S., and Weber, A.P. (2012). Molecular crosstalk between PAMP-triggered immunity and photosynthesis. Mol. Plant Microbe Interact. **25**:1083–1092.

Grigorova, B., Mara, C., Hollender, C., Sijacic, P., Chen, X., and Liu, Z. (2011). LEUNIG and SEUSS co-repressors regulate miR172 expression in *Arabidopsis* flowers. Development **138**:2451–2456.

Guan, D., Yan, B., Thieme, C., Hua, J., Zhu, H., Boheler, K.R., Zhao, Z., Kragler, F., Xia, Y., and Zhang, S. (2017). PlaMoM: a comprehensive database compiles plant mobile macromolecules. Nucleic Acids Res. **45**:D1021–D1028.

Han, X., Kumar, D., Chen, H., Wu, S., and Kim, J.Y. (2014). Transcription factor-mediated cell-to-cell signalling in plants. J. Exp. Bot. **65**:1737–1749.

Hauri, S., Comoglio, F., Seimiya, M., Gerstung, M., Glatter, T., Hansen, K., Aebersold, R., Paro, R., Gstaiger, M., and Beisel, C. (2016). A high-density map for navigating the human polycomb complexome. Cell Rep. **17**:583–595.

Heitz, T., Widemann, E., Lugan, R., Miesch, L., Ullmann, P., Desaubry, L., Holder, E., Grausem, B., Kandel, S., Miesch, M., et al. (2012). Cytochromes P450 CYP94C1 and CYP94B3 catalyze two successive oxidation steps of plant hormone jasmonoyl-isoleucine for catabolic turnover. J. Biol. Chem. **287**:6296–6306.

Henras, A.K., Plisson-Chastang, C., O'Donohue, M.F., Chakraborty, A., and Gleizes, P.E. (2015). An overview of pre-ribosomal RNA processing in eukaryotes. Wiley Interdiscip. Rev. RNA **6**:225–242.

Henras, A.K., Soudet, J., Gerus, M., Lebaron, S., Caizergues-Ferrer, M., Mougin, A., and Henry, Y. (2008). The post-transcriptional steps of eukaryotic ribosome biogenesis. Cell Mol Life Sci **65**:2334–2359.

Hillmer, R.A., Tsuda, K., Rallapalli, G., Asai, S., Truman, W., Papke, M.D., Sakakibara, H., Jones, J.D.G., Myers, C.L., and Katagiri, F. (2017). The highly buffered *Arabidopsis* immune signaling network conceals the functions of its components. PLoS Genet. **13**:e1006639.

Hoehenwarter, W., Monchgesang, S., Neumann, S., Majovsky, P., Abel, S., and Muller, J. (2016). Comparative expression profiling reveals a role of the root apoplast in local phosphate response. BMC Plant Biol. **16**:106.

Horstman, A., Fukuoka, H., Muino, J.M., Nitsch, L., Guo, C., Passarinho, P., Sanchez-Perez, G., Immink, R., Angenent, G., and Boutilier, K. (2015). AIL and HDG proteins act antagonistically to control cell proliferation. Development **142**:454–464.

Huang, D., Wu, W., Abrams, S.R., and Cutler, A.J. (2008). The relationship of drought-related gene expression in *Arabidopsis thaliana* to hormonal and environmental factors. J. Exp. Bot. **59**:2991–3007.

Huang da, W., Sherman, B.T., and Lempicki, R.A. (2009). Systematic and integrative analysis of large gene lists using DAVID bioinformatics resources. Nat. Protoc. **4**:44–57.

Ishida, T., Maekawa, S., and Yanagisawa, S. (2016). The pre-rRNA processing complex in *Arabidopsis* includes two WD40-domain-containing proteins encoded by glucose-inducible genes and plant-specific proteins. Mol. Plant **9**:312–315.

Jang, G., Lee, S., Chang, S.H., Kim, J.K., and Choi, Y.D. (2018). Jasmonic acid modulates xylem development by controlling polar auxin transport in vascular tissues. Plant Biotechnol. Rep. **12**:265–271.

Jia, H.F., Chai, Y.M., Li, C.L., Lu, D., Luo, J.J., Qin, L., and Shen, Y.Y. (2011). Abscisic acid plays an important role in the regulation of strawberry fruit ripening. Plant Physiol. **157**:188–199.

Kanei, M., Horiguchi, G., and Tsukaya, H. (2012). Stable establishment of cotyledon identity during embryogenesis in *Arabidopsis* by ANGUSTIFOLIA3 and HANABA TARANU. Development **139**:2436–2446.

Kasahara, H. (2016). Current aspects of auxin biosynthesis in plants. Biosci. Biotechnol. Biochem. **80**:34–42.

Kitaoka, N., Matsubara, T., Sato, M., Takahashi, K., Wakuta, S., Kawaide, H., Matsui, H., Nabeta, K., and Matsuura, H. (2011). *Arabidopsis* CYP94B3 encodes jasmonyl-L-isoleucine 12-hydroxylase, a key enzyme in the oxidative catabolism of jasmonate. Plant Cell Physiol **52**:1757–1765.

Kong, A.T., Leprevost, F.V., Avtonomov, D.M., Mellacheruvu, D., and Nesvizhskii, A.I. (2017). MSFragger: ultrafast and comprehensive peptide identification in mass spectrometry-based proteomics. Nat. Methods **14**:513–520.

Koo, A.J., Cooke, T.F., and Howe, G.A. (2011). Cytochrome P450 CYP94B3 mediates catabolism and inactivation of the plant hormone jasmonoyl-L-isoleucine. Proc. Natl. Acad. Sci. U S A **108**:9298–9303.

Koo, A.J., Thireault, C., Zemelis, S., Poudel, A.N., Zhang, T., Kitaoka, N., Brandizzi, F., Matsuura, H., and Howe, G.A. (2014). Endoplasmic reticulum-associated inactivation of the hormone jasmonoyl-L-isoleucine by multiple members of the cytochrome P450 94 family in *Arabidopsis*. J. Biol. Chem. **289**:29728–29738.

Krogan, N.J., Cagney, G., Yu, H., Zhong, G., Guo, X., Ignatchenko, A., Li, J., Pu, S., Datta, N., Tikuisis, A.P., et al. (2006). Global landscape of protein complexes in the yeast *Saccharomyces cerevisiae*. Nature **440**:637–643.

Kumar, L., and Futschik, M. (2007). Mfuzz: a software package for soft clustering of microarray data. Bioinformation **2**:5–7.

Kunkel, B.N., and Harper, C.P. (2018). The roles of auxin during interactions between bacterial plant pathogens and their hosts. J. Exp. Bot. **69**:245–254.

Kustatscher, G., Grabowski, P., Schrader, T.A., Passmore, J.B., Schrader, M., and Rappsilber, J. (2019). Co-regulation map of the human proteome enables identification of protein functions. Nat. Biotechnol. **37**:1361–1371.

Lan, P., Li, W., and Schmidt, W. (2012). Complementary proteome and transcriptome profiling in phosphate-deficient *Arabidopsis* roots reveals multiple levels of gene regulation. Mol. Cell Proteomics **11**:1156–1166.

Lee, J.H., Terzaghi, W., Gusmaroli, G., Charron, J.B., Yoon, H.J., Chen, H., He, Y.J., Xiong, Y., and Deng, X.W. (2008). Characterization of *Arabidopsis* and rice DWD proteins and their roles as substrate receptors for CUL4-RING E3 ubiquitin ligases. Plant Cell **20**:152–167.

Lee, J.H., Yoon, H.J., Terzaghi, W., Martinez, C., Dai, M., Li, J., Byun, M.O., and Deng, X.W. (2010). DWA1 and DWA2, two *Arabidopsis* DWD protein components of CUL4-based E3 ligases, act together as negative regulators in ABA signal transduction. Plant Cell **22**:1716–1732.

Leon-Reyes, A., Van der Does, D., De Lange, E.S., Delker, C., Wasternack, C., Van Wees, S.C., Ritsema, T., and Pieterse, C.M. (2010). Salicylate-mediated suppression of jasmonate-responsive gene expression in *Arabidopsis* is targeted downstream of the jasmonate biosynthesis pathway. Planta **232**:1423–1432.

Li, J., Brader, G., and Palva, E.T. (2004). The WRKY70 transcription factor: a node of convergence for jasmonate-mediated and salicylate-mediated signals in plant defense. Plant Cell **16**:319–331.

Liu, X., Li, Y., and Zhong, S. (2017). Interplay between light and plant hormones in the control of *Arabidopsis* seedling chlorophyll biosynthesis. Front. Plant Sci. **8**:1433.

Lopez-Molina, L., Mongrand, S., Kinoshita, N., and Chua, N.H. (2003). AFP is a novel negative regulator of ABA signaling that promotes ABI5 protein degradation. Genes Dev. **17**:410–418.

Lynch, T.J., Erickson, B.J., Miller, D.R., and Finkelstein, R.R. (2017). ABI5-binding proteins (AFPs) alter transcription of ABA-induced genes via a variety of interactions with chromatin modifiers. Plant Mol. Biol. **93**:403–418.

Mano, Y., and Nemoto, K. (2012). The pathway of auxin biosynthesis in plants. J. Exp. Bot. **63**:2853–2872.

Meng, X., Zhou, J., Tang, J., Li, B., de Oliveira, M.V.V., Chai, J., He, P., and Shan, L. (2016). Ligand-induced receptor-like kinase complex regulates floral organ abscission in *Arabidopsis*. Cell Rep. **14**:1330–1338.

Merchante, C., Stepanova, A.N., and Alonso, J.M. (2017). Translation regulation in plants: an interesting past, an exciting present and a promising future. Plant J. **90**:628–653.

Mergner, J., Frejno, M., List, M., Papacek, M., Chen, X., Chaudhary, A., Samaras, P., Richter, S., Shikata, H., Messerer, M., et al. (2020). Mass-spectrometry-based draft of the *Arabidopsis* proteome. Nature **579**:409–414.

Mine, A., Nobori, T., Salazar-Rondon, M.C., Winkelmuller, T.M., Anver, S., Becker, D., and Tsuda, K. (2017). An incoherent feed-forward loop mediates robustness and tunability in a plant immune network. EMBO Rep. **18**:464–476.

Missbach, S., Weis, B.L., Martin, R., Simm, S., Bohnsack, M.T., and Schleiff, E. (2013). 40S ribosome biogenesis co-factors are essential for gametophyte and embryo development. PLoS One **8**:e54084.

Mordret, E., Dahan, O., Asraf, O., Rak, R., Yehonadav, A., Barnabas, G.D., Cox, J., Geiger, T., Lindner, A.B., and Pilpel, Y. (2019). Systematic detection of amino acid substitutions in proteomes reveals mechanistic basis of ribosome errors and selection for translation fidelity. Mol. Cell **75**:427–441 e425.

Muller, T.M., Bottcher, C., and Glawischnig, E. (2019). Dissection of the network of indolic defence compounds in *Arabidopsis thaliana* by multiple mutant analysis. Phytochemistry **161**:11–20.

Müller, J.B., Geyer, P.E., Colaço, A.R., Treit, P.V., Strauss, M.T., Oroshi, M., Doll, S., Virreira Winter, S., Bader, J.M., Köhler, N., et al. (2020). The proteome landscape of the kingdoms of life. Nature **582**:592–596.

Nakashima, K., Takasaki, H., Mizoi, J., Shinozaki, K., and Yamaguchi-Shinozaki, K. (2012). NAC transcription factors in plant abiotic stress responses. Biochim. Biophys. Acta **1819**:97–103.

Navarro, L., Dunoyer, P., Jay, F., Arnold, B., Dharmasiri, N., Estelle, M., Voinnet, O., and Jones, J.D. (2006). A plant miRNA contributes to antibacterial resistance by repressing auxin signaling. Science **312**:436–439.

Nee, G., Kramer, K., Nakabayashi, K., Yuan, B., Xiang, Y., Miatton, E., Finkemeier, I., and Soppe, W.J.J. (2017). DELAY OF GERMINATION1 requires PP2C phosphatases of the ABA signalling pathway to control seed dormancy. Nat. Commun. **8**:72.

Nickstadt, A., Thomma, B.P.H.J., Feussner, I., Kangasjarvi, J., Zeier, J., Loeffler, C., Scheel, D., and Berger, S. (2004). The jasmonate-insensitive mutant jin1 shows increased resistance to biotrophic as well as necrotrophic pathogens. Mol. Plant Pathol. **5**:425–434.

Obayashi, T., Hayashi, S., Saeki, M., Ohta, H., and Kinoshita, K. (2009). ATTED-II provides coexpressed gene networks for *Arabidopsis*. Nucleic Acids Res. **37**:D987–D991.

Paez Valencia, J., Goodman, K., and Otegui, M.S. (2016). Endocytosis and endosomal trafficking in plants. Annu. Rev. Plant Biol. **67**:309–335.

Patharkar, O.R., and Walker, J.C. (2016). Core mechanisms regulating developmentally timed and environmentally triggered abscission. Plant Physiol. **172**:510–520.

Patharkar, O.R., and Walker, J.C. (2018). Advances in abscission signaling. J. Exp. Bot. **69**:733–740.

Patterson, S.E., and Bleecker, A.B. (2004). Ethylene-dependent and -independent processes associated with floral organ abscission in *Arabidopsis*. Plant Physiol. **134**:194–203.

Pieterse, C.M., Van der Does, D., Zamioudis, C., Leon-Reyes, A., and Van Wees, S.C. (2012). Hormonal modulation of plant immunity. Annu. Rev. Cell Dev. Biol. **28**:489–521.

Pino, L.K., Searle, B.C., Bollinger, J.G., Nunn, B., MacLean, B., and MacCoss, M.J. (2020). The Skyline ecosystem: Informatics for quantitative mass spectrometry proteomics. Mass Spectrom. Rev. **39**:229–244.

Ponnala, L., Wang, Y., Sun, Q., and van Wijk, K.J. (2014). Correlation of mRNA and protein abundance in the developing maize leaf. Plant J. **78**:424–440.

Qi, L., Yan, J., Li, Y., Jiang, H., Sun, J., Chen, Q., Li, H., Chu, J., Yan, C., Sun, X., et al. (2012). *Arabidopsis thaliana* plants differentially modulate auxin biosynthesis and transport during defense responses to the necrotrophic pathogen *Alternaria brassicicola*. New Phytol. **195**:872–882.

Robatzek, S., Chinchilla, D., and Boller, T. (2006). Ligand-induced endocytosis of the pattern recognition receptor FLS2 in *Arabidopsis*. Genes Dev. **20**:537–542.

Rogers, H., and Munne-Bosch, S. (2016). Production and scavenging of reactive oxygen species and redox signaling during leaf and flower senescence: similar but different. Plant Physiol. **171**:1560–1568.

Rounds, C.M., and Bezanilla, M. (2013). Growth mechanisms in tip-growing plant cells. Annu. Rev. Plant Biol. **64**:243–265.

Schweizer, F., Fernandez-Calvo, P., Zander, M., Diez-Diaz, M., Fonseca, S., Glauser, G., Lewsey, M.G., Ecker, J.R., Solano, R., and Reymond, P. (2013). *Arabidopsis* basic helix-loop-helix transcription factors MYC2, MYC3, and MYC4 regulate glucosinolate biosynthesis, insect performance, and feeding behavior. Plant Cell **25**:3117–3132.

Sherp, A.M., Westfall, C.S., Alvarez, S., and Jez, J.M. (2018). *Arabidopsis thaliana* GH3.15 acyl acid amido synthetase has a highly specific substrate preference for the auxin precursor indole-3-butyric acid. J. Biol. Chem. **293**:4277–4288.

Shim, J.S., Jung, C., Lee, S., Min, K., Lee, Y.W., Choi, Y., Lee, J.S., Song, J.T., Kim, J.K., and Choi, Y.D. (2013). AtMYB44 regulates WRKY70 expression and modulates antagonistic interaction between salicylic acid and jasmonic acid signaling. Plant J. **73**:483–495.

Skinner, O.S., and Kelleher, N.L. (2015). Illuminating the dark matter of shotgun proteomics. Nat. Biotechnol. **33**:717–718.

Smirnova, E., Marquis, V., Poirier, L., Aubert, Y., Zumsteg, J., Menard, R., Miesch, L., and Heitz, T. (2017). Jasmonic acid oxidase 2 hydroxylates jasmonic acid and represses basal defense and resistance responses against *Botrytis cinerea* infection. Mol. Plant **10**:1159–1173.

Smyth, D.R., Bowman, J.L., and Meyerowitz, E.M. (1990). Early flower development in *Arabidopsis*. Plant Cell **2**:755–767.

Soltanieh, S., Lapensee, M., and Dragon, F. (2014). Nucleolar proteins Bfr2 and Enp2 interact with DEAD-box RNA helicase Dbp4 in two different complexes. Nucleic Acids Res. **42**:3194–3206.

Song, G., Hsu, P.Y., and Walley, J.W. (2018). Assessment and refinement of sample preparation methods for deep and quantitative plant proteome profiling. Proteomics **18**:e1800220.

Song, S.K., Hofhuis, H., Lee, M.M., and Clark, S.E. (2008). Key divisions in the early *Arabidopsis* embryo require POL and PLL1 phosphatases to establish the root stem cell organizer and vascular axis. Dev. Cell **15**:98–109.

Song, Y., Xiang, F., Zhang, G., Miao, Y., Miao, C., and Song, C.P. (2016). Abscisic acid as an internal integrator of multiple physiological processes modulates leaf senescence onset in *Arabidopsis thaliana*. Front. Plant Sci. **7**:181.

Spoel, S.H., Johnson, J.S., and Dong, X. (2007). Regulation of tradeoffs between plant defenses against pathogens with different lifestyles. Proc. Natl. Acad. Sci. U S A **104**:18842–18847.

Spoel, S.H., Koornneef, A., Claessens, S.M., Korzelius, J.P., Van Pelt, J.A., Mueller, M.J., Buchala, A.J., Metraux, J.P., Brown, R., Kazan, K., et al. (2003). NPR1 modulates cross-talk between salicylate- and jasmonate-dependent defense pathways through a novel function in the cytosol. Plant Cell **15**:760–770.

Staswick, P.E., and Tiryaki, I. (2004). The oxylipin signal jasmonic acid is activated by an enzyme that conjugates it to isoleucine in *Arabidopsis*. Plant Cell **16**:2117–2127.

Stenvik, G.E., Butenko, M.A., Urbanowicz, B.R., Rose, J.K., and Aalen, R.B. (2006). Overexpression of INFLORESCENCE DEFICIENT IN ABSCISSION activates cell separation in vestigial abscission zones in *Arabidopsis*. Plant Cell **18**:1467–1476.

Su, J., Yang, L., Zhu, Q., Wu, H., He, Y., Liu, Y., Xu, J., Jiang, D., and Zhang, S. (2018). Active photosynthetic inhibition mediated by MPK3/MPK6 is critical to effector-triggered immunity. PLoS Biol. **16**:e2004122.

Sugawara, S., Hishiyama, S., Jikumaru, Y., Hanada, A., Nishimura, T., Koshiba, T., Zhao, Y., Kamiya, Y., and Kasahara, H. (2009). Biochemical analyses of indole-3-acetaldoxime-dependent auxin biosynthesis in *Arabidopsis*. Proc. Natl. Acad. Sci. U S A **106**:5430–5435.

Szklarczyk, D., Gable, A.L., Lyon, D., Junge, A., Wyder, S., Huerta-Cepas, J., Simonovic, M., Doncheva, N.T., Morris, J.H., Bork, P., et al. (2019). STRING v11: protein-protein association networks with increased coverage, supporting functional discovery in genome-wide experimental datasets. Nucleic Acids Res. **47**:D607–D613.

Szymanski, J., Levin, Y., Savidor, A., Breitel, D., Chappell-Maor, L., Heinig, U., Topfer, N., and Aharoni, A. (2017). Label-free deep shotgun proteomics reveals protein dynamics during tomato fruit tissues development. Plant J. **90**:396–417.

Takasaki, H., Maruyama, K., Takahashi, F., Fujita, M., Yoshida, T., Nakashima, K., Myouga, F., Toyooka, K., Yamaguchi-Shinozaki, K., and Shinozaki, K. (2015). SNAC-As, stress-responsive NAC transcription factors, mediate ABA-inducible leaf senescence. Plant J. **84**:1114–1123.

Teale, W.D., Paponov, I.A., and Palme, K. (2006). Auxin in action: signalling, transport and the control of plant growth and development. Nat. Rev. Mol. Cell Biol. **7**:847–859.

Thieme, C.J., Rojas-Triana, M., Stecyk, E., Schudoma, C., Zhang, W., Yang, L., Minambres, M., Walther, D., Schulze, W.X., Paz-Ares, J., et al. (2015). Endogenous *Arabidopsis* messenger RNAs transported to distant tissues. Nat. Plants **1**:15025.

Thimm, O., Blasing, O., Gibon, Y., Nagel, A., Meyer, S., Kruger, P., Selbig, J., Muller, L.A., Rhee, S.Y., and Stitt, M. (2004). MAPMAN: a user-driven tool to display genomics data sets onto diagrams of metabolic pathways and other biological processes. Plant J. **37**:914–939.

Tran, L.S., Nakashima, K., Sakuma, Y., Simpson, S.D., Fujita, Y., Maruyama, K., Fujita, M., Seki, M., Shinozaki, K., and Yamaguchi-Shinozaki, K. (2004). Isolation and functional analysis of *Arabidopsis* stress-inducible NAC transcription factors that bind to a drought-responsive *cis*-element in the early responsive to dehydration stress 1 promoter. Plant Cell **16**:2481–2498.

Truman, W.M., Bennett, M.H., Turnbull, C.G., and Grant, M.R. (2010a). *Arabidopsis* auxin mutants are compromised in systemic acquired resistance and exhibit aberrant accumulation of various indolic compounds. Plant Physiol. **152**:1562–1573.

Truman, W.M., Bennett, M.H., Turnbull, C.G.N., and Grant, M.R. (2010b). *Arabidopsis* auxin mutants are compromised in systemic

acquired resistance and exhibit aberrant accumulation of various indolic compounds. Plant Physiol. **152**:1562–1573.

Tsuda, K., Sato, M., Glazebrook, J., Cohen, J.D., and Katagiri, F. (2008). Interplay between MAMP-triggered and SA-mediated defense responses. Plant J. **53**:763–775.

Tyanova, S., Temu, T., Sinitcyn, P., Carlson, A., Hein, M.Y., Geiger, T., Mann, M., and Cox, J. (2016). The Perseus computational platform for comprehensive analysis of (prote)omics data. Nat. Methods **13**:731–740.

Van der Does, D., Leon-Reyes, A., Koornneef, A., Van Verk, M.C., Rodenburg, N., Pauwels, L., Goossens, A., Korbes, A.P., Memelink, J., Ritsema, T., et al. (2013). Salicylic acid suppresses jasmonic acid signaling downstream of SCFCOI1-JAZ by targeting GCC promoter motifs via transcription factor ORA59. Plant Cell **25**:744–761.

Walley, J.W., Sartor, R.C., Shen, Z., Schmitz, R.J., Wu, K.J., Urich, M.A., Nery, J.R., Smith, L.G., Schnable, J.C., Ecker, J.R., et al. (2016). Integration of omic networks in a developmental atlas of maize. Science **353**:814–818.

Wan, C., Borgeson, B., Phanse, S., Tu, F., Drew, K., Clark, G., Xiong, X., Kagan, O., Kwan, J., Bezginov, A., et al. (2015). Panorama of ancient metazoan macromolecular complexes. Nature **525**:339–344.

Wang, X., Gao, J., Zhu, Z., Dong, X., Wang, X., Ren, G., Zhou, X., and Kuai, B. (2015). TCP transcription factors are critical for the coordinated regulation of isochorismate synthase 1 expression in *Arabidopsis thaliana*. Plant J. **82**:151–162.

Wang, Y., Li, L., Ye, T., Lu, Y., Chen, X., and Wu, Y. (2013). The inhibitory effect of ABA on floral transition is mediated by ABI5 in *Arabidopsis*. J. Exp. Bot. **64**:675–684.

Waters, M.T., and Langdale, J.A. (2009). The making of a chloroplast. EMBO J. **28**:2861–2873.

Weis, B.L., Kovacevic, J., Missbach, S., and Schleiff, E. (2015). Plant-specific features of ribosome biogenesis. Trends Plant Sci. **20**:729–740.

Widemann, E., Miesch, L., Lugan, R., Holder, E., Heinrich, C., Aubert, Y., Miesch, M., Pinot, F., and Heitz, T. (2013). The amidohydrolases IAR3 and ILL6 contribute to jasmonoyl-isoleucine hormone turnover and generate 12-hydroxyjasmonic acid upon wounding in *Arabidopsis* leaves. J. Biol. Chem. **288**:31701–31714.

Wisniewski, J.R., Hein, M.Y., Cox, J., and Mann, M. (2014). A "proteomic ruler" for protein copy number and concentration estimation without spike-in standards. Mol. Cell Proteomics **13**:3497–3506.

Wojciechowska, N., Marzec-Schmidt, K., Kalemba, E.M., Zarzynska-Nowak, A., Jagodzinski, A.M., and Bagniewska-Zadworna, A. (2018). Autophagy counteracts instantaneous cell death during seasonal senescence of the fine roots and leaves in *Populus trichocarpa*. BMC Plant Biol. **18**:260.

Woldemariam, M.G., Onkokesung, N., Baldwin, I.T., and Galis, I. (2012). Jasmonoyl-L-isoleucine hydrolase 1 (JIH1) regulates jasmonoyl-L-isoleucine levels and attenuates plant defenses against herbivores. Plant J. **72**:758–767.

Wrzaczek, M., Brosche, M., Salojarvi, J., Kangasjarvi, S., Idanheimo, N., Mersmann, S., Robatzek, S., Karpinski, S., Karpinska, B., and Kangasjarvi, J. (2010). Transcriptional regulation of the CRK/DUF26 group of receptor-like protein kinases by ozone and plant hormones in *Arabidopsis*. BMC Plant Biol. **10**:95.

Wu, F., Chi, Y., Jiang, Z., Xu, Y., Xie, L., Huang, F., Wan, D., Ni, J., Yuan, F., Wu, X., et al. (2020). Hydrogen peroxide sensor HPCA1 is an LRR receptor kinase in *Arabidopsis*. Nature **578**:577–581.

Yadeta, K.A., Elmore, J.M., Creer, A.Y., Feng, B., Franco, J.Y., Rufian, J.S., He, P., Phinney, B., and Coaker, G. (2017). A cysteine-rich protein kinase associates with a membrane immune complex and the cysteine residues are required for cell death. Plant Physiol. **173**:771–787.

Ye, H., Liu, S., Tang, B., Chen, J., Xie, Z., Nolan, T.M., Jiang, H., Guo, H., Lin, H.Y., Li, L., et al. (2017). RD26 mediates crosstalk between drought and brassinosteroid signalling pathways. Nat. Commun. **8**:14573.

Yi, S.Y., Shirasu, K., Moon, J.S., Lee, S.G., and Kwon, S.Y. (2014). The activated SA and JA signaling pathways have an influence on flg22-triggered oxidative burst and callose deposition. PLoS One **9**:e88951.

Zander, M., Thurow, C., and Gatz, C. (2014). TGA transcription factors activate the salicylic acid-suppressible branch of the ethylene-induced defense program by regulating ORA59 expression. Plant Physiol. **165**:1671–1683.

Zhang, C., Lei, Y., Lu, C., Wang, L., and Wu, J. (2020). MYC2, MYC3, and MYC4 function additively in wounding-induced jasmonic acid biosynthesis and catabolism. J. Integr. Plant Biol. **62**:1159–1175.

Zhang, H., Liu, P., Guo, T., Zhao, H., Bensaddek, D., Aebersold, R., and Xiong, L. (2019). *Arabidopsis* proteome and the mass spectral assay library. Sci. Data **6**:278.

Zhang, M., Yuan, B., and Leng, P. (2009). The role of ABA in triggering ethylene biosynthesis and ripening of tomato fruit. J. Exp. Bot. **60**:1579–1588.

Zhang, T., Poudel, A.N., Jewell, J.B., Kitaoka, N., Staswick, P., Matsuura, H., and Koo, A.J. (2016). Hormone crosstalk in wound stress response: wound-inducible amidohydrolases can simultaneously regulate jasmonate and auxin homeostasis in *Arabidopsis thaliana*. J. Exp. Bot. **67**:2107–2120.

Zheng, X.Y., Spivey, N.W., Zeng, W., Liu, P.P., Fu, Z.Q., Klessig, D.F., He, S.Y., and Dong, X. (2012). Coronatine promotes *Pseudomonas syringae* virulence in plants by activating a signaling cascade that inhibits salicylic acid accumulation. Cell Host Microbe **11**:587–596.

Zheng, X.Y., Zhou, M., Yoo, H., Pruneda-Paz, J.L., Spivey, N.W., Kay, S.A., and Dong, X. (2015). Spatial and temporal regulation of biosynthesis of the plant immune signal salicylic acid. Proc. Natl. Acad. Sci. U S A **112**:9166–9173.

Ziegler, J., Qwegwer, J., Schubert, M., Erickson, J.L., Schattat, M., Burstenbinder, K., Grubb, C.D., and Abel, S. (2014). Simultaneous analysis of apolar phytohormones and 1-aminocyclopropan-1-carboxylic acid by high performance liquid chromatography/electrospray negative ion tandem mass spectrometry via 9-fluorenylmethoxycarbonyl chloride derivatization. J. Chromatogr. A. **1362**:102–109.